João Tiago Soares Henriques

Bachelor in Micro and Nanotechnologies Engineering

1D Fiber-shaped supercapacitors

Dissertation for obtaining the Master's Degree in

Engineering of Micro and Nanotechnologies

Supervisor: Doctor Ana Catarina Bernardino Baptista, Researcher, CENIMAT|I3N, NOVA University of Lisbon

Co-Supervisor: Doctor Isabel Maria Mercês Ferreira, Associate Professor, NOVA University of Lisbon

Examination Committee

Chair: Doctor Rodrigo Ferrão de Paiva Martins, Full Professor, NOVA University of Lisbon

Rapporteurs: Doctor Luís Miguel Nunes Pereira, Invited Associate Professor, NOVA University of Lisbon

Members: Doctor Ana Catarina Bernardino Baptista, Researcher, NOVA University of Lisbon

October de 2021

FACULDADE DE CIÊNCIAS E TECNOLOGIA
UNIVERSIDADE NOVA DE LISBOA

1D Fiber-shaped Supercapacitors

Aos meus pais, por todo o apoio e dedicação.

Acknowledgments

The presented work would not have been possible without the help and contribution of everyone involved, from institutional parties to friends and family. Thus, I would like to thank first to my advisor Prof. Dr. Ana Baptista for the opportunity to develop my masters on the biocompatible fiber-shaped supercapacitors, and the patience, dedication, and support, given to me throughout my master's progression. I also thank my co-advisor Prof. Dr. Isabel Ferreira for all the patience, and help provided throughout the masters. I appreciate all my adviser and co-advisor advise, suggestions, and the cheer up, given to me for the extra boost needed to get back on track, when everything seemed to go wrong. For all of this and for the great masters experience that Prof. Dr. Ana Baptista and Prof. Dr. Isabel Ferreira provided me, I have nothing else to say but that I'm very grateful.

I thank my former co-worker Nuno Lima for starting the work on biocompatible fiber-shaped supercapacitors and for all the time dedicated to share and explain his previous results from his master and from the developed work as a member of Prof. Dr. Isabel research team. Even after leaving the academic world Nuno still shown to be available for my student questions. Thank you for guiding me though the labs on the first weeks and for sharing your methods on your device constitution and characterization. It really gave me a good strong start.

João, aka Joãozinho, I am grateful for your help and guidance on the Gamry software and for all the time you spent with me explaining the data analysis mechanisms. I also thank you for your availability to help me and to clarify my abundant questions during the experimental work.

I thank PhD students, David, and Jaime for all the help and guidance on the labs and all the helpful advice and company during the long lab days. I appreciate a lot your patience and friendly approach to my master student doubts and comments.

I thank my fellow master students Andreia, Iris, Miguel and Sofia for the friendship and joy that was the lab work alongside with you guys. You really helped me cheering up throughout the master's progression, turning the sometimes-boring work into a pleasant experience. I really liked to meet and work alongside with you.

To my old-time course friends, André Violas, Célia Rocha, Luís Araújo, Rui Guilhôto and João Durand, I specially thank you for all the amazing 5 years of friendship, trust, and shared experience. It has been a pleasure to experience with you this life-time adventure that is the academic world and all the related matter. Particularly for me, an insular student that traveled alone something like 600 Atlantic Ocean miles, to an unknown place with very few known people. It was a very exciting and stimulating experience but a very frightening one to. This way, I was very lucky to have such amazing people like you guys to go along with me and I really hope that this friendship lasts as much as we do. Regarding to the master's experience, I thank all of you for the cheer up and availability to help me every time that I needed. You were just impeccable. I would like to particularly thank Célia for all the strength and motivation given to me during this master and for not giving up on me, always trying to help, despite my stubbornness. Thank you, Célia. I appreciate all your effort and dedication to make me a better person and I will try to return the same level of dedication and kindness to you.

A very important pilar throughout my life journey was, an always will be my family, with a special place for my mother and father. I'm eternally grateful to you for the big effort that was raising me, for always be there, for the trust, for the dedication, care, nurturing, and for everything that you did to make me what I am today. And of course, I thank you for funding my studies, with special tanks for the master's degree that I am finishing with this document. You really gave everything and even more than in cold ask or desire, and still do, even though I can mostly take

care of myself. Beyond everything else I was blessed with your support and guidance that lead me to what I am now and to complete this master's degree. That is something with a priceless value that I do not know how to address with words but need to mention. I specially thank my father for the time and energy spend to motivate me with his wise advice to take my studies further with this master's degree. Without his persistence it probably would never become a reality. And I specialty thank my mother for the company and good food during my university student days. There is nothing like mothers' food to cheer up during the difficult times.

I thank my cousin Antelmo Gonçalves for all these years of an amazing friendship and for helping me during these master's years. You were my salvation on the first academic years. It helped a lot to have a known trustworthy person alongside me at that time and I really needed it. It was a pleasure to daily share with you the university experience. It was sad and disconcerting when you had to go back to the island. Still, even at the distance you support me and continued to make me feel more like home. I thank you for everything and I hope to be always present on your life to. And I thank all the good talks and outdoor activities we had the opportunity to do on this last year. It helps to maintain a clear and sane mind.

I thank my cousin Afonso Pereira, who is also working on his master's degree in computing science, for all the support, experience sharing, and all those good resting times, gaming or exercising at the park to clear the mind and the ideas. Those change of air were heavily needed, and it is always pleasant to spend some good time with an old-time fellow like you. Thank for all your support and presence.

Finally, I thank all my family for the support and care that gave me the mind set and wellbeing to face the daily life challenge. And for those I did not mention, that helped and take part on this journey in a way or another, I left here a final warm thank.

This work was supported by national funds through the project "All-Fibre Integrated Photovoltaic Storage Device for e-Textiles, with reference PTDC/CTM-CTM/1571/2020.

Abstract

Nowadays, exponential technological advances, allied with contemporary mass globalization, drove humankind to a whole new world of possibilities and specialized solutions, able to answer our daily challenges of all life aspects. An example of these new technological solutions is the emerging intelligent textiles, best known as wearables or e-clothes, capable of enhancing daily garments, by adding new revolutionary functionalities.

In this work, it will be presented three new configurations of energy storage devices (supercapacitors) based on already studied textile materials [1], especially suitable for wearable electronics applications. The presented configurations, namely, the braid-like, the woven, and the mesh-like configuration, have commercial carbon threads as electrodes and share a simulated sweat solution electrolyte since these devices were designed to work with user sweat. For the separation layer, electrospun cellulose acetate nanofibers were used in the braid-like and the mesh-like configurations, and a hydrophilic felt for the woven one. Moreover, electrode functionalization with polypyrrole (PPy) was carried out, showing considerable results in the device performance enhancement. Regarding the electrical study, cyclic voltammetry and cyclic charge-discharge experiments were the primary characterization technics. Additionally, washability and cyclic charge-discharge endurance (for 1000 cycles) were addressed for the two most successful configuration (the brain-like and internally woven configurations). The electrical characterization showed promising results, estimating 0.62 $F.g^{-1}$ for the most successful device (replica 3 from internally woven configuration) and one order of magnitude enhancement with electrodes functionalization step. Moreover, the washability study proven the supercapacitors (the brain-like and internally woven configurations) ability to maintain most of its electrical performance after 5 washing cycles, with special highlights for the internally woven configuration that maintain more than 80% of its initial specific capacitance for both studied replicas. Additionally, electrodes PPy functionalization's quality and assembling processes proven to be the key points for devices success.

Resumo

Nos dias que correm, os avanços tecnológicos exponenciais, aliados à atual globalização em massa, conduziram a humanidade a um novo mundo de possibilidades e soluções especializadas, capazes de responder aos nossos desafios diários em todos os aspetos da vida. Um exemplo das referidas novas soluções tecnológicas são os emergentes têxteis inteligentes, mais conhecidos como *wearables* ou *e-clothes*, capazes de valorizar a indumentaria diária, adicionando-lhe novas funcionalidades revolucionárias.

Neste trabalho, serão apresentadas 3 novas configurações de dispositivos de armazenamento de energia (supercondensadores). Estas baseiam-se em materiais têxteis já estudados [1], especialmente adequados para aplicações em eletrónica vestível. As 3 configurações, apresentadas neste trabalho, são respetivamente a configuração tipo trança, a tecida e a configuração tipo grade. Todas elas utilizam fios de carbono comerciais como elétrodo e partilham o mesmo eletrólito, baseado numa solução de suor simulado [2], uma vez que estes dispositivos foram projetados para trabalhar com o suor do utilizador. Relativamente á camada separadora, para as configurações em forma de trança e tipo grade, esta foi alcançada por electrofiação de nano fibras de acetato de celulose. Já para a configuração tecida, foi utilizado um pedaço de tecido de feltro hidrofílico para o mesmo fim. Posteriormente, para as configurações mais bem-sucedidas (configuração tipo trança e internamente tecida), foi realizada a funcionalização dos elétrodos utilizando polipirrol (PPy). Relativamente ao estudo do comportamento elétrico, as técnicas de voltametria cíclica e carga-descarga cíclica foram as principais técnicas de caracterização utilizadas. Adicionalmente, a capacidade de lavagem e a resistência à carga-descarga cíclica (para 1000 ciclos) foram testadas para as duas configurações de maior sucesso. A caracterização elétrica apresentou resultados promissores, estimando 0,62 $F.g^{-1}$ para o melhor dispositivo e demonstrando um aumento de uma ordem de grandeza, na capacitância especifica, com a funcionalização dos elétrodos. Aliado a este resultado, o estudo de lavagens dos dispositivos demonstrou a capacidade dos mesmos para reter grande parte da sua capacitância especifica, ao fim de 5 ciclos de lavagem. Em destaque ficou a configuração internamente tecida, que manteve mais de 80% da sua capacitância especifica original, ao fim dos 5 ciclos de lavagem. Finalmente, a qualidade da funcionalização dos elétrodos com PPy e o processo de montagem dos dispositivos, revelaram-se os principais fatores para o sucesso dos mesmos.

Contents

List of Tables

List of Figures

Acronyms

CA	Cellulose Acetate
CCD	Cyclic Charge-Discharge
CV	Cyclic Voltammetry
CPs	Conductive Polymers
ESD	Energy storage device
EDL	Electric doble layer
EDLC	Electric doble-layer capacitor
PANI	Polyaniline
PPy	Polypyrrole
PTh	Polythiophene
SC	Specific Capacitance
SR	Scan-Rate
SSS	Simulated Sweat Solution

Symbols

A	Area
C	Capacitance
C_4H_5N	Pyrrole
E_d	Energy density
ε	Permittivity
ε_0	Vacuum permittivity
$FeCl_3$	Iron Chloride
I	Current
P_d	Power density
Q	Charge
m	Mass
V	Voltage

Motivation and Objectives

One of today's biggest concerns, faced by humanity, is energy production and storage, to respond to the growing worldwide demand [3]. Beyond other things, this is related with the exponential use of electronic devices that helps and ease our daily life [4]. A particular electronic device group that already has a strong presence in the modern lifestyle are wearable devices [5]. Due to their versatility and wide range applicability on people life needs, wearables are believed to have soaring presence and impact on our day-to-day life on the near future. Because of this, wearable technology is already attracting the attention of technological companies that are investing a lot of capital and time on its development [6].

Although wearables are a very promising technology, there are still some challenges waiting to be solved. Even though flexible and bendable electronics are already available, flexible and bendable energy storage devices (ESDs) are still limited to low energy and power density and shortened lifespan [4], [7]. This fact represents a great barrier for wearables development and implementation, especially for the e-clothes concept, that stands for interactive clothing. This futuristic clothing kind are believed to be able to perform useful tasks like monitoring vital signals, real time body checkups, adapt to the environment condition, between others [6], [8], [9]. Moreover, the e-clothes concept requires flexible, cheap, biocompatible, and reliable energy storage devices. Therefore, the research community have been taking efforts in finding ingenious architectures that fulfil the listed features.[10]–[13] . Following these trends, the objective of this thesis is the production of 1D energy storage devices suitable for clothes, focusing the assemble and characterization of said devices, using flexible and biocompatible materials. More specifically, carbon yarns will play the electrodes role, and electrospun cellulose acetate nanofibers and hydrophilic felt fabric will be used as the separator layer for different configurations. Moreover, the carbon electrodes will be functionalized with Polypyrrole (PPy), adding the electrode´s available surface area and contributing to the device performance with a pseudocapacitive behavior [14], [15]. Regarding the electrolyte, the built supercapacitors will use synthetic simulated sweat solution (SSS) as electrolyte to easily compare the results with previous work [1].

1 Introduction

1.1 Wearable energy devices applications and architectures

As many times before, humanity is facing a new change in day-to-day life. Nowadays, due to the contemporary mass globalization, allied with the exponential technological advances in all areas of knowledge, humankind have never lived days with such an immensity of possibilities and solutions to respond and overcome daily situations. Whether at work, in personal life, or any other life aspect, technology is always around to support us, sometimes without even being noticed[16][8]. One recent technology that has been gaining more and more relevance are wearable electronics. This game changing concept aims to integrate electronics in everyday wearables, adding useful new functions to them, following the nowadays demand for utility and functionality[5], [6], [17]. As displayed in **Figure 1.1**, wearable gadgets can be implemented in any common garments, as well as in occasional or more technical habits and outfits, thus highlighting its technology versatility [18][9]. To reach this reality, flexible, conformable, and light weight devices, with a similar lifespan to its non-intelligent counterparts are mandatory. In response, 1D, 2D, and 3D structures have been investigated and presented as spotlighted architectures to accomplish wearables conception[7], [11], [12], [19].

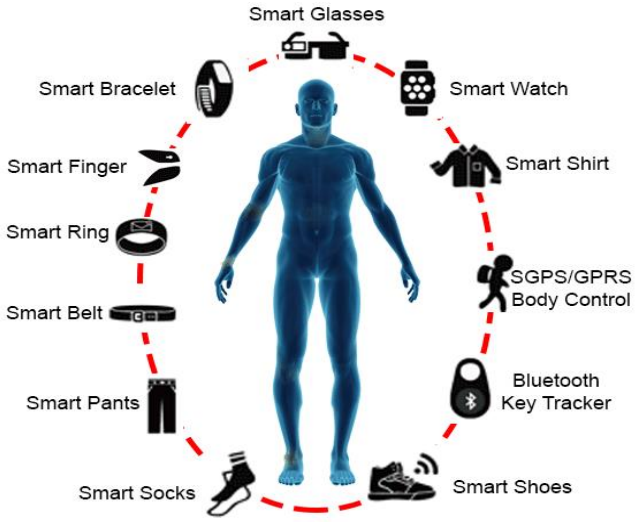

Figure 1.1 - Illustration of possible wearable application for daily use. From [8]

Regarding 1D architectures, fiber-shaped devices have shown promising results to get the most of e-clothes technology, once fiber represents the base of most garments, enabling direct weaving instead of traditional externally integrated devices in clothes [6] [20] [1]. One of the most common 1D fiber approaches present a coaxial structure (core-shell design) with inner and outer electrodes separated from an ion conductive layer (active layer). These outlines can be repeated to form multilayer fibers with boosted performance. Twisted arrangement is another frequent approach in 1D architectures due to its simplicity and proven results, with its electrodes twisted together and separated by coating one of them with an active layer [4] [21]. Nevertheless, recent research presented novel 1D approaches that rises from breeding together coaxial and twisted configuration, as well as align nanotubes, anchored on a conductive substrate (**Figure 1.2**, **1D**), for wearable energy harvesting devices, energy storage devices, and hybrid devices (energy harvesting and storage device) [4], [21]–[23]. Additionally, either metal-based, polymer-based or carbonaceous nanomaterial-based, 1D architecture is characterized by its conformability, flexibility, and light wight, making it highly suitable for adaptable e-clothes [11] [1], [4], [10], [20]–[23]. Stepping up one dimension, energy harvesting and storage devices with 2D architectures shown to be very popular as well on intelligent garments matter. Usually, these configurations result from the planarization of device electrodes and separation layer (ion conductive

layer) with low thickness to ensure flexibility. For this reason, 2D architecture highly benefit from the exploration of 2D materials (also suitable for 1D and 2D architectures), like graphene [24], transition metal oxides [25], black phosphorus [26], and others, taking advantage of its characteristic properties, namely planer electric and thermic conduction and flexibility due to their thin thicknesses [3][9][18]. Finally, sponge-like 3D structures profit from the porous nature of some bulk materials to achieve flexible bulk devices, with high electrodes surface area, when soaked in electrolyte [27] [28]. This way, porous bulky structures can accumulate mechanical strain and still achieve considerable charge accumulation and high power-density, making this architecture suitable for wearable batteries and supercapacitors. Such structures are achieved via flexible conductive polymers (CPs), flexible matrices like PDMS, and\or graphene frameworks. Engineered in flexible and porous substrates like paper and others, these devices are assemble through three main processes, namely, self-assembly, template assisted and direct deposition methods) as described by *Cao et al* [29]. Nonetheless, recent studies shown methods for 3D printed devices and its characteristics which reveal a significant assemble method for 3D, 2D and 1D wearable devises [7], [30]. **Figure 1.2** illustrates some examples of wearable energy storage and harvesting devices for the three discussed architectures.

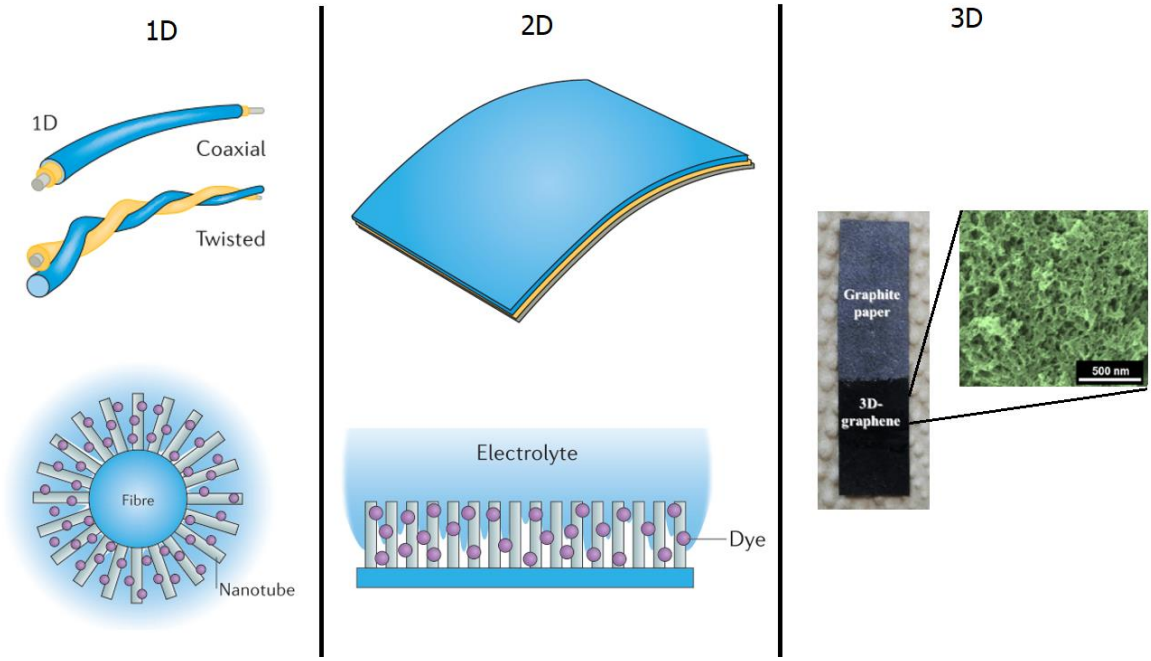

Figure 1.2 - Illustration of 1D, 2D [4] and 3D [28] architectures of wearable energy storage and harvest devices.

Furthermore, even though each architecture presents its strengths for specific applications, in overview, 1D devices have currently gain more and more relevance for textile applications. Particularly, energy storage devices like fiber-shaped supercapacitor, due to their noticeable characteristics, namely flexibility, low weight, highly compatibility with already running garments manufacturing processes, with remarkable electrical performance, distinguishable for its high power-density and fast charge-discharge cycles with a considerable lifespan. Additionally, new ecofriendly approaches based on carbon electrodes, cellulosic material for the dielectric layer, aqueous electrolytes (liquid and polymer gel electrolytes), and garment base substrates like cotton, are presented as very suitable devices for sustainable large-scale production, responding to the contemporary environmental urge [1], [10], [31]. One remarkable example of eco-friendly fiber shaped supercapacitor is the device presented by *Lima et al.* [1] reaching a specific capacity of 2.3 $F.g^{-1}$ and 386.5 $mWh.kg^{-1}$ and 46.4 $kW.kg^{-1}$ energy-density (E_d) and power-density (P_d) respectively. Notwithstanding, wearable energy harvesting and storage devices still present drawbacks like, limited mechanical durability, poor electrical conductivity, and restrained lifespan (compared to traditional ones). Therefore, many research efforts have been conducted to counteract these wearable weaknesses and help to create market level products.

1.2 Capacitor's storage ability and characterization

Capacitors represent a family of electronic component with the ability to store charge. They differ from batteries due to their primary electrostatic physical nature in contrast with batteries electrochemical character. Therefore, capacitors are distinguished by their fast charge-discharge cycle, wide lifespan, low E_d, and wider operation temperatures [32], [33]. Moreover, with the last century scientific developments, capacitors reach a new level of maturation, giving birth to new device categories, namely electrostatic capacitors, electrolytic capacitors, electric double-layer capacitors (EDLC), and pseudocapacitors, according to their constitution, operating principle, and capacitance. For energy storage device purpose, the last two categories are highlighted due to their higher E_d and P_d values [13], [14], [34], [35]. The capacitor's ability to store charge is described by its capacitance (*C*) which is the physical entity that relates the potential difference (V) needed to store a certain amount of charge (Q in Coulombs), for a particular capacitor, as displayed in Eq 1.1. Capacitance only depends on capacitors materials (mainly its dielectric material) and geometry, being measured in Farads (*F*) [33].

$$C = \frac{Q}{V} \qquad \text{Eq 1.1}$$

Since capacitance depends on capacitor geometry and material, its equation alters with device architecture and functional material. As example, for parallel plated capacitors, capacitance can be written thought **Equation 1.2**, where A is the electrode area, ε the permittivity constant of dielectric material, d the distance between electrodes, and ε_0 is the vacuum permittivity [33].

$$C = \frac{\varepsilon\, \varepsilon_0\, A}{d} \qquad \text{Eq 1.2}$$

Although capacitance is very useful to characterize capacitors, in real life application it is more useful the determination of the capacitance per unit measure of a specific quantity. This way, specific capacitance (SC) is commonly used to the referred end. Moreover, it is usually written as the capacitance per area unit or per mass unit as it will be addressed in this work. Through **Equation 2.1** and **Equation 2.2** it is possible to calculate the resulting SC form cyclic voltammetry (CV) and cyclic charge-discharge experiments (CCD) experiments respectively. In these equation $\frac{C}{m}$ is the specific capacitance, m is one electrode mass, ν is the scan-rate (SR), ΔV the voltage window, $I_{(V)}$ is the resulting current from the CV measurement [1] and I is the applied current during the CCD performance.

$$\frac{C}{m} = \frac{1}{m\, \nu\, \Delta V} \int I_{(V)} dV \qquad \text{Eq 2.1}$$

$$\frac{C}{m} = \frac{I\, \Delta t}{m\, \Delta V} \qquad \text{Eq 2.2}$$

Other important characteristics to complement energy storage devices description are the Energy density (quantification of the energy amount on a particular system in $Wh\, Kg^{-1}$) and power density (quantization of the amount of work energy in a system in $W\, Kg^{-1}$). For this, **Equation 3** and **Equation 4** can be used to describe the referred supercapacitors characteristics [1].

$$E_d = \frac{C\, (\Delta V)^2}{2} \qquad \text{Eq 3}$$

$$P_d = \frac{E}{t} = \frac{I\, \Delta V}{2} \qquad \text{Eq 4}$$

1.2.1 Supercapacitors and charge accumulation mechanisms

Supercapacitors represent a class of capacitor distinguished by their remarkable capacitance. This is achieved by two main charge accumulation mechanism, namely the electrical doble layer formation and the pseudocapacitance method [13], [14], [31], [32], [34], [35]. The first method is engineered by immersing the electrodes on a dielectric medium (liquid or gel format). This results in ionic adsorption on the electrode surface, mainly with its opposite charge, that continuously extends throughout the dielectric medium. Consequently it is generated an electrical potential that fads with the distance d, from the electrode, as described by German Physicist Otto Stern [36]. In this scenario, the adsorbed ions contribute to stabilize the accumulated charge (on the electrode) and raise its number due to the stronger electrical potential formed. Such device is illustrated in **Figure 1.3 a)** [31]. Moreover, the greater the electrode surface area, the greater the amount of charge accumulated [13], [37]. Thereby, as displayed in **Figure 1.3 d)** and **e)**, devices with this charge accumulation mechanism used materials like activated carbon to enhance its electrodes active surface area.

On the other hand, pseudocapacitors are attained using electrochemically active material on the capacitor's electrodes, that store charge via fast reversible surface redox reaction (Faradic charge transfer) [10], [13] as shown in **Figure 1.3 b)** [31]. For this to happened, electrodes material needs a high chemical affinity with the adsorbed ions from the capacitor's dielectric medium, as well as a high specific area to maximize said redox reactions. Such materials can be divided into two main groups, namely transition metal oxides like MnO_2, ZnO, FeO_3, so on, and electric conductive polymers like polyaniline (PANI), polypyrrole (PPy), polythiophene (PTh), polyvinyl alcohol (PVA), etc [34][15]. Moreover, hybrid capacitors (devices with asymmetric electrodes, where each electrode have one of the two discussed charge storage mechanism, as shown in **Figure 1.3 c)**) have been a research focus due to their considerable power density and energy density values. These devices show promising results, maintain the supercapacitors high P_d, granted by its electrostatic electrode, and raises its E_d through its electrochemical electrode, getting out the best of both worlds.

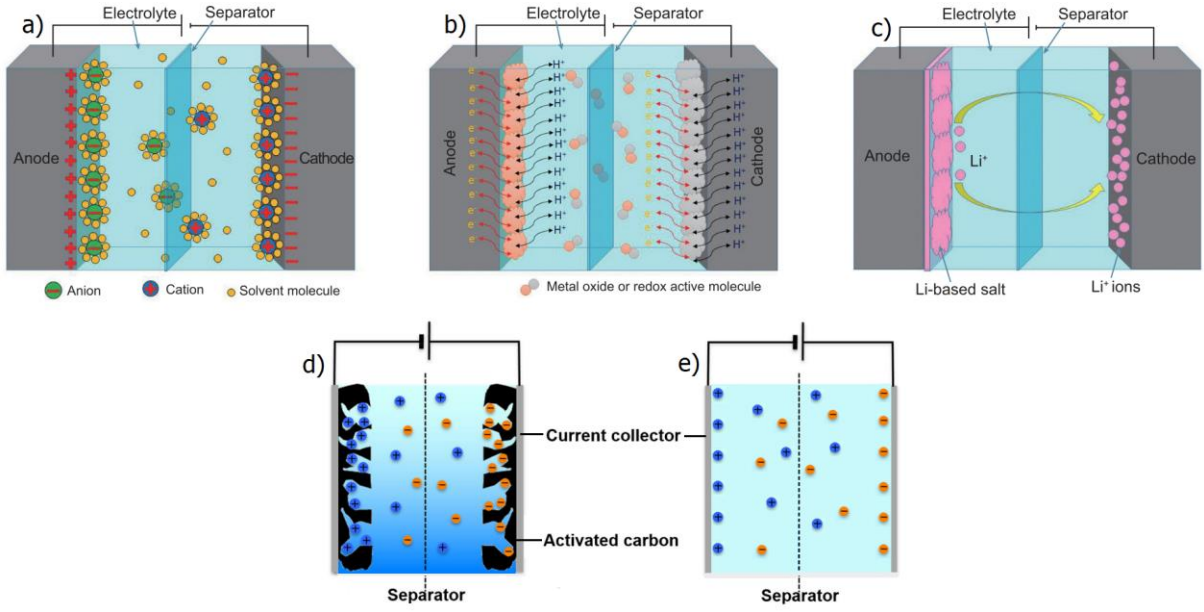

Figure 1.3 - Working mechanism ilustration of a) EDLC, b) pseudocapacitor, C) asymmetric capacitor (from *Chen et al.* [31]), followed by a synthetic representation of electrodes specific area influence d) on a high specific area electrode (like active carbon), and e) a flat surface electrode, adapted form *Kado et al.* [35].

1.3 State of the Art

The first register of a capacitive device goes back to 1745 by the physicist Ewald von Kleist, where he reports having experienced an electric shock wile touching a metallic wire inside a glass bottle of water, held by him, that had been previously charge with a generator. Despite its incomplete explanation of the event, it did not go unnoticed and later, in 1746, physicist Pieter van Musschenbroek used a similar setup to create what is known by the Leyden jar [38]. Henceforth, the device was developed, resulting into nowadays wide variety of energy storage devices called capacitors. For wearable ESDs, supercapacitors are highlighted due to their superior E_d, P_d, flexibility, and cyclic performance, hance effort has been made on their development[5], [6], [13], [14], [17], [34].

A determining component on supercapacitors performance is the electrode, therefore, most of the research attention is focused on its development. Into this subject, carbonaceous materials (carbon threads, activated carbon, carbon-nanotubes, graphene, and graphite) have been highlighted due to their remarkable capacitance, electric conductivity, flexibility, chemical bonding diversity and structural integrity[14], [34], [35], [39]. Carbon-based electrode supercapacitors are predominantly EDL devices due to their electrostatic nature, conferring high cyclic lifespan [14]. However, composite electrodes represent an alternative carbon application onto pseudocapacitive electrodes[35]. On this arrangement, carbon acts as a secondary material to add conductivity, structural integrity or even act like a structural scaffold [14]. To reach the full potential of carbon-based supercapacitors, high purity electrodes with a controlled porous size are required, elsewise, electrodes conductivity and effective surface area will be compromised, degrading device performance [14], [31]. Furthermore, the required methods to produce such electrodes, have associated high costs, limiting carbon-based electrode's performance economic-wise. Regarding pseudocapacitive supercapacitors, metal-oxide and conductive polymer electrodes are the leading materials [10], [13], [34]. Particularly, MnO_2 have been heavily studied as pseudocapacitive electrode material mainly due to its relative low cost and high theoretical SC (around 1370 F g^{-1} [40]). For polymer electrodes, PPy, PANI and PTh are the go-to materials mainly because of their considerable conductivity, easy and cheap synthesis, high capacitance, and environmental stability [13], [15]. Moreover, contrary to most CPs, PPy is reported to have high cycling stability, making it very promising for wearable electrode material [15]. Given their electrochemical nature, metal-oxide and polymer electrodes present higher E_d. However, lower electrode conductivity, slower charge-discharge rate, and shorter cyclic life (being the last one more prevalent in polymer electrodes due to the mechanic strain created by ion insertion/desertion on the polymer chains[13]) are presented as the pseudocapacitive device downfall, when compared with its EDLC counterparts [14], [15]. This way, as stated before, researcher's attention is focused on breeding pseudocapacitive material with carbon to overcome the referred weaknesses and create supercapacitors suitable for wearable needs. Appendix **Table 4** displays the main performance results presented in some research work on supercapacitors for wearable applications as well as the most successful devices developed in this work.

Concerning ESDs electrolytes, **Equation 1.2** reveals its impact on device capacitance, increasing with electrolyte permittivity and thin thickness. Usually strong acids and bases (H_2SO_4 and KOH respectively) are used for ESDs electrolyte [31], [35], yet, for wearable applications, hazard substances must be substituted for biocompatible solutions like aqueous solutions and polymer gel, to respond market safety requirements [10]. The big issue lays on maintain a considerable electrode/electrolyte affinity using biocompatible electrolytes. Another solution is to encapsulate the devices while using dangerous electrolytes, however, garment wight, lake of breathability, and electrolyte leakage risk, make it unsuitable for user comfort and safety. *Lima et al.* [1] presented a suitable solution, with its 1D biocompatible supercapacitor, using sweat as electrolyte, PPy functionalized carbon threads as electrodes and electrospun CA non-woven fibers as separator layer. Additionally, wearable ESDs can be constructed on flexible substrates, like fabrics and flexible polymers, that usually works as encapsulation and/or separator material.

2 Materials and Methods

2.1 Device configuration

In this work, three 1D supercapacitors' configurations were assembled and studied, namely the braid-like, the woven, and the mesh-like configurations. Regarding the braid-like architecture, a twisted approaches, presented by *Lima et al.* [1] was also assembled and tested to compare both approaches, as displayed in **Figure 2.1 a)** and **b)** respectively. These two electrode devices, featured commercially carbon thread electrodes (from TENAX, 218 Ω/m) with 10 cm, coated with PPy that enhanced its electrochemical performance. The dielectric layer, where the electrolyte is adsorbed, was achieved by CA electrospun fibers around one of the two electrodes. The twisted devices assembly consisted in manually twisting the outer electrode (PPy polymerized carbon thread) around the inner electrode (PPy polymerized carbon thread with a deposition of CA electrospun fiber). For the braid configuration, the PPy polymerized outer electrode was split in two halves and manually braided around the also PPy polymerized and CA electrospun coated inner electrode. These configurations were initially assembled without PPy coating to be used as control device and the braid-like configuration was electrically tested afterwards due to its mechanical enhanced mechanical stability.

For the woven configuration, 3 different electrode dispositions were studied, sharing the same basic structure, namely, two carbon yarns (that function as electrodes) manually woven into a piece of hydrophilic felt fabric. As displayed in **Figure 2.1 c), d)** and **e),** parallel internal electrodes, parallel external electrodes, and crossed electrodes where experimented. Furthermore, the internal woven electrodes were later assembled and tested, using PPy coated carbon yarns, given their performing superiority. The final devices featured 7 cm PPy coated yarns internally woven in a 1.5 cm × 3 cm hydrophilic cotton fabric.

Additionally, the mesh-like structure was experimented, and it consisted in weaving carbon yarns through CA electrospun coated carbon yarns, alternately as shown in **Figure 2.1 f)**. Annex **Figure B. 4** displays photos of each assembled devices configuration.

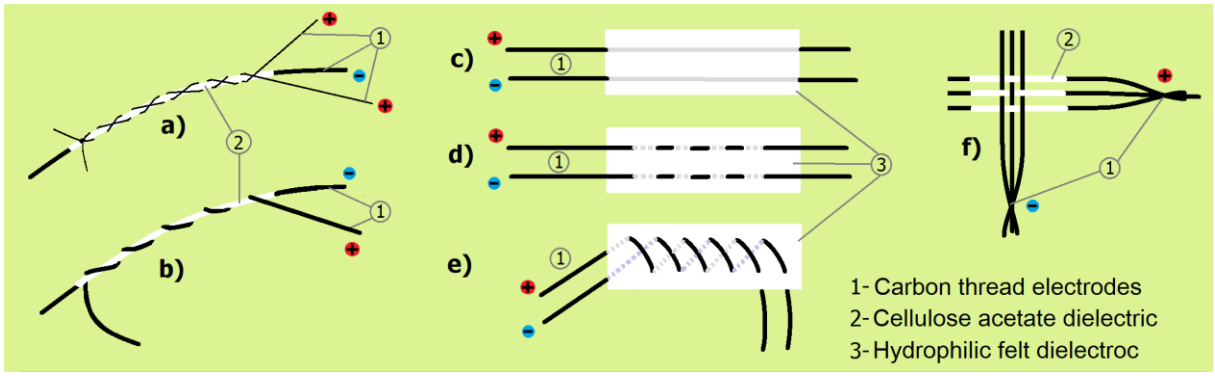

Figure 2.1 – Representative models of the assembled 1D devices configuration. Braid-like and twisted-like configurations are represented in **a)** and **b)** respectively.Parallel internal, external and crossed woven configurations are peresent in **c)**, **d)** and **e)** respectively, and mesh-like configuration is displyed in **f)**.

2.2 Electrospun CA fibers

The electrospun nanofibers, used as the separator layer on the braid-like devices, were attained using a 12% CA solution (Mn = 50,000 with 40% acetyl groups, Sigma-Aldrich) with acetone (LABCHEM) and dimethylacetamide (CARLO ERBA), in a 2:1 wt ratio, as solvents. For the electrospinning process, the solution was loaded into a 1 mm syringe with a 21 gauged needle tip (from ITEC). The carbon yarns were the target of this process and were disposed vertically aligned on a plastic

frame as shown in **Figure B. 1** present in the appendix B. The process was made in ambient condition with controlled temperature and humidity (around 22 ºC and 40% humidity) during 45 minutes on both sides of the yarns, being the process total time of 90 minutes. The pumping rate of the solution was 0.2 mL/h and the potential applied between the needle and the target was between 18 kV to 19 kV.

2.3 PPy polymerization method

For the commercially carbon yarns functionalization, it was performed *in situ* polymerization of pyrrole (C_4H_5N, M_w = 67.09 g.mol^{-1}, purity = 98%, Sigma-Aldrich). For this, iron chloride hexahydrate ($FeCl_3.6H_2O$, Sigma Aldrich) was used as the oxidizing agent. The first step of the polymerization process was to immerse the carbon thread (13 cm to 15 cm of the carbon yarn full length of 20 cm) on a 0.05 M aqueous pyrrole solution for 10 min. Then, it was slowly added an iron chloride hexahydrate aqueous solution, with a monomer to oxidizer ratio of 2. The reaction time used was 20h. Note that before immersing the carbon yarn, it should be cleaned with current water and conventional dish soap to take out residual grease or other sub products, resulting from its industrial production and storage, thar cold be on the carbon threads, affecting the polymerization. Other important step after immersing the carbon thread on the pyrrole solution, is to let it there for 15 minutes, enable the monomer to be adsorbed onto the carbon thread filaments to ensure that the polymerization takes place on the threads surface evenly.

Finally, after taking the threads out of the solution, they were immersed on ethanol to stop possible remaining ongoing reaction and the excess PPy was cleaned with current water.

2.4 Electrolyte preparation and method of use

The electrolyte used to test the achieved devices was a simulated sweat solution (SSS) with a pH of 5.5. This aqueous solution contained sodium chloride (Sigma Aldrich, 99.5%), sodium phosphate monobasic (Fluka analytical, 90%) and L-histidine (Sigma Aldrich, 99%) respectively in 0.5%, 0.22% and 0.05% of wt/v, according to reference [2].

All devices were tested in electrolyte saturated condition. For this, in braid-like configuration, it was used 45 µL of SSS while in the woven configurations 500 µL were needed.

2.5 Electrical characterization

To electrically characterize the devices, CV and CCD assays were performed on a potentiostat (model Gamry Instruments-Reference 3000). Initially, the double electrode devices were characterized skipping the electrodes PPy polymerization. For this device, CV was performed using a sweep voltage window of 1V (from -0.5 V to 0.5 V) on five different scan-rates (10 mV/s, 20 mV/s, 50 mV/s, 100 mV/s and 200 mV/s). Relatively to the CCD experiments it was used a charge voltage from 0 V to 0.5 V followed by discharge voltage form 0.5 V to 0 V, with five different charge-discharge currents (5 µA, 10 µA, 15 µA, 20 µA and 25 µA). PPy coated electrodes device were tested in a similar way, using, for the CV, a sweep voltage window from -1 V to 1V on four different scan-rates (50 mV/s, 100 mV/s, 200 mV/s and 400 mV/s). The CCD was performed using a charge voltage up to 1 V and discharge voltage down to 0 V, with six different charge-discharge currents (50 µA, 75 µA, 100 µA, 150 µA, 200 µA, 300 µA). Though **Equation 2.1** and **Equation 2.2**, present on the Introduction chapter, the specific capacity of each device was estimated. For this, the accumulated charge and sweep voltage window were evaluated using the devise CV curves on Gamry Echem Analyst ™ software. For the calculation of the SC it was considered the mass of a single carbon electrode for the non-polymerized devices, and the mass of the PPy-functionalized carbon fiber for functionalized devices.

2.6 Morphological characterization

Electrodes surface morphology was studied thought scanning electron microscopy (SEM) (model Hitachi S2400 Scanning Electron Microscope) using a gold-palladium sample coating. The samples were disposed in a sample holder, using conductive carbon tape.

3 Results and Discussion

Following the processes described on the previous sections, the braid-like, woven, and mesh-like configurations where electrically tested. For this, the study started with simpler devices that featured only carbon yarns as electrodes, and CA separation layer, further adding the PPy functionalization on the most successful configurations. This way it was possible to save some time and resources on the process as well as study the electrochemical impact of the PPy coating. In other to better organize and present the attained information, this section will be divided in three main subsections, namely the PPy polymerization method, the braid-like configuration and the woven configurations and the mesh-like configuration.

3.1 Polymerization study

One determining step on the production of the proposed supercapacitors on this thesis is the PPy polymerization step. With this process, device electrochemical ability is greatly enhanced as shown in reference [1]. The reason behind this enhancement can be explained with the increase on the electrodes surface area and the added insertion/decorations charge accumulation mechanism, inherent to CPs and PPy in this case [13], [32]. On the other hand, this is the most time-consuming process on the devices production since it takes 20 hours of polymerization plus initial preparation and final wash of the excess aggregated polymer [1]. Having in mind the importance of this step, an initial optimization study was performed. Thus, PPy polymerization on carbon yarns was performed throughout different process times, namely 3 h, 5 h, 8 h, and 20 h of PPy polymerization. After washing and drying the polymerized threads, a multimeter was used to measure the yarns resistance, where its tips were 1 cm apart, contacting the coated yarn section. Considerable differences were observed, with a prevalent increase of resistance for longer polymerization time. Knowing that PPy has higher resistivity than carbon threads and the higher the resistance of a polymerized thread, thicker the PPy coating, 20 h polymerization process was maintained, since it was shown the best results on PPy coating evenness and thickness. Moreover, devices with the 20h polymerization coating process presented better electrical performance (for both CV and CCD tests). To complete this information, SEM analyses were performed on the threads with different polymerization times. Through the SEM images present in **Figure 3.1** was possible to observe that the PPy is coating the carbon electrode surface, however no significant difference on the uniformity of PPy coating is observed for the different polymerization time. The polymerization of 20 h was selected due to its smoother appearance.

Other optimization attempt targeted the number of resulting coated yarns in each process, through a multi yarn polymerization experiment. Regarding the setup, the threads were vertically disposed, inside a container with the polymerization precursors, externally hanged as showed in **Figure 3.1**. Although promising, this polymerization setup was not used on the final work because of 2 main issues that mutually contribute for abandoning this setup. The first challenge of this multi yarn polymerization was related with the precursor solution volume. Since each 10 cm yarn should have between 6 cm to 7 cm of coated length, it was needed a high aspect ratio container to have approximately 7 cm of precursor solution depth, using the proportional quantities calculated from the reference [1]. This condition result in bringing the yarns closer together during the polymerization process which caused the formation of PPy bridges between yarns. Consequently, it led to an uneven PPy coating and its strip off, during the PPy excess cleaning process. In short, the yarns had to be placed further apart, however, by doing it, a bigger precursor solution volume was needed, turning the polymerization process more expensive per coated yarn. This way, it was decided to stick with the polymerization process described in the literature [1].

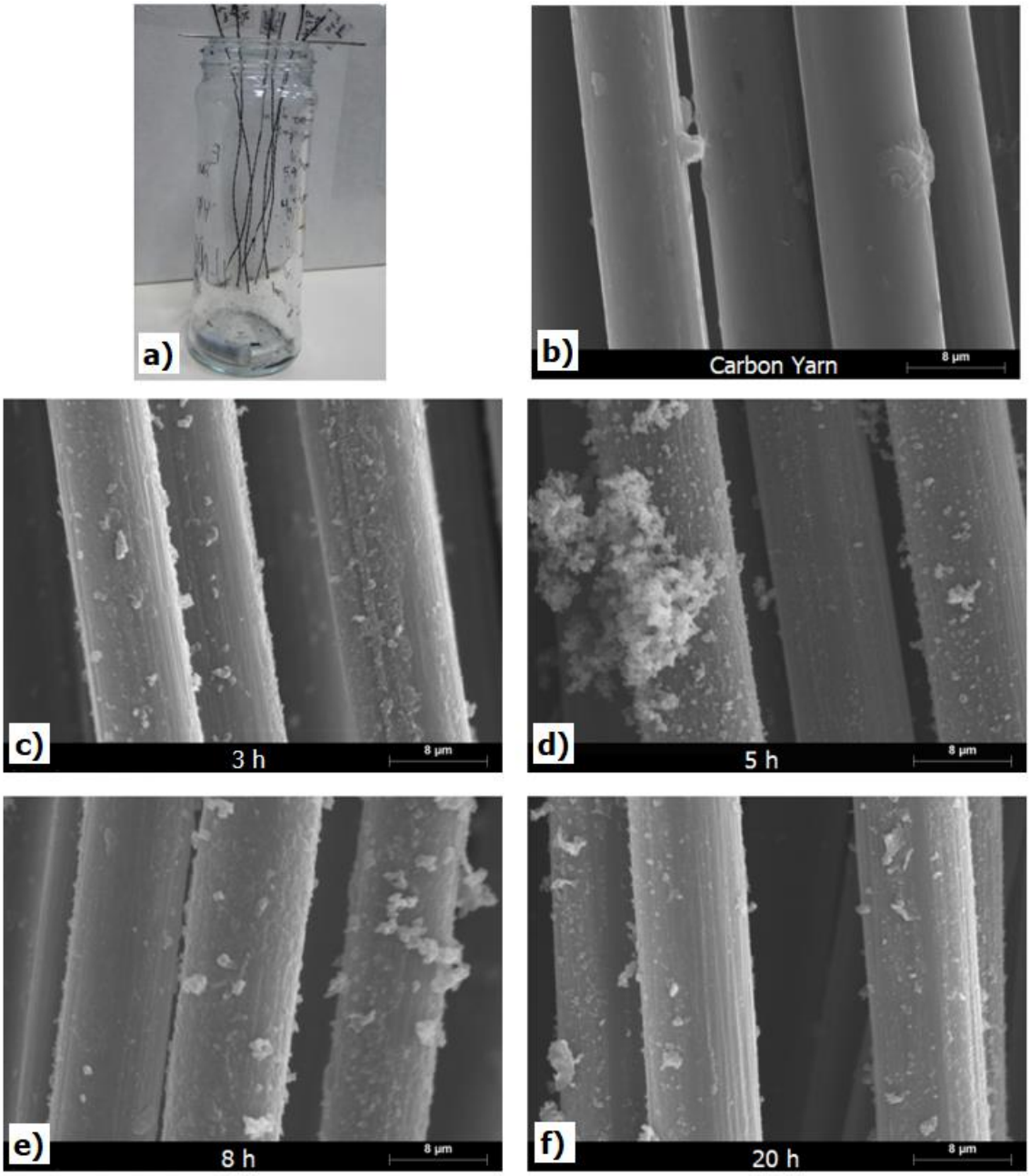

Figure 3.1 - Photography of multi-yarn polymerization setup a). SEM images with 4000x magnification and 20KV of uncoated carbon yarn b) and coated with the c) 3 h, d) 5 h, e) 8 h and f) 20 h of polymerization.

3.2 Braid-like configuration

Initially, the braid-like configuration study was started by reproducing the fiber shaped device presented by *Lima et al.* [1]. As described on Materials and Methods section, this device was achieved by twisting a PPy coated carbon yarn around another equivalent yarn with an additional electrospun CA layer. This way, the two carbon yarns, function as the supercapacitor electrodes and the electrospun CA layer as the electrical insulator between the contacts, where the electrolyte is absorbed. Although impressive results were attained on the referred work, there were still some possible improvements to the presented device configuration, such as the improvement of contact area between the outer electrode and insulating layer, and the enhancement of washing resistance of the outer electrode. This way, it was assembled a similar 1D fiber shaped device with the outer electrode disposed in a braid-like configuration around the CA electrospun electrode. For this, the outer electrode (PPy coated carbon

yarn) was divided in two and braid around the second electrode as shown is **Figure 2.1**. The objective was to achieve a wider contact area between the CA layer and the outer electrode (up to the double) maintaining the same number of turns presented in *Lima et al.* work. It should be noted that the twisted configuration presented in *Lima et al.* was also assembled. However, the maximum number of turs achieved with it, stayed at 9 turns which left a wide unused area on the device. Furthermore, maintaining the twisted configuration stable was challenging, since the outer electrode tended to unfold, due to the built tangential strain, during the twisting process. This way, the braid configuration was able to ease the unfolding problem, enabling to tie the outer electrode with a knot at the end of the braiding process and reducing the tangential strain of the outer electrode. With the braided device assembled, its electrical performance was initially evaluated, using only carbon yarns as electrodes and electrospun CA as separator layer (skipping the polymerization step). The objective of this was to evaluate the possibility of using a simpler arrangement for an energy storage device and further examine the impact of the polymerization step on the device's electrical response.

3.2.1 Devices without PPy coated electrodes

On the first stage of braid-like device study, it was performed cyclic voltammetry using 10 cycles of each tested scan rates, namely 10 mV/s, 20 mV/s, 50 mV/s, 100 mV/s and 200 mV/s. The SSS electrolyte was added using a micropipette to apply the 45 µL referred on *Materials and methods* section. **Figure 3.2** shows, on the left, the CV results, from the 9th cycle of each experiment, as well as the SR vs SC graphic on the right. In this figure, it is possible to see that, for the tested scan-rates, the device CV curve presents a quasi-rectangular shape characteristic of electrical double layer formation on the capacitors electrodes [1], [41]. Regarding the SR vs SC relation, the lowest scan-rates testes result in the higher specific capacity. This behavior can be explained with the fact that, for lower rates, the contributing energy storage ions and charges have more time to move and accumulate on the device electrodes [41]. Other important observation on the CV curves is that, within the experimented scan-rates, each cycle resulted in a similar curve, suggesting the device electrochemical stability.

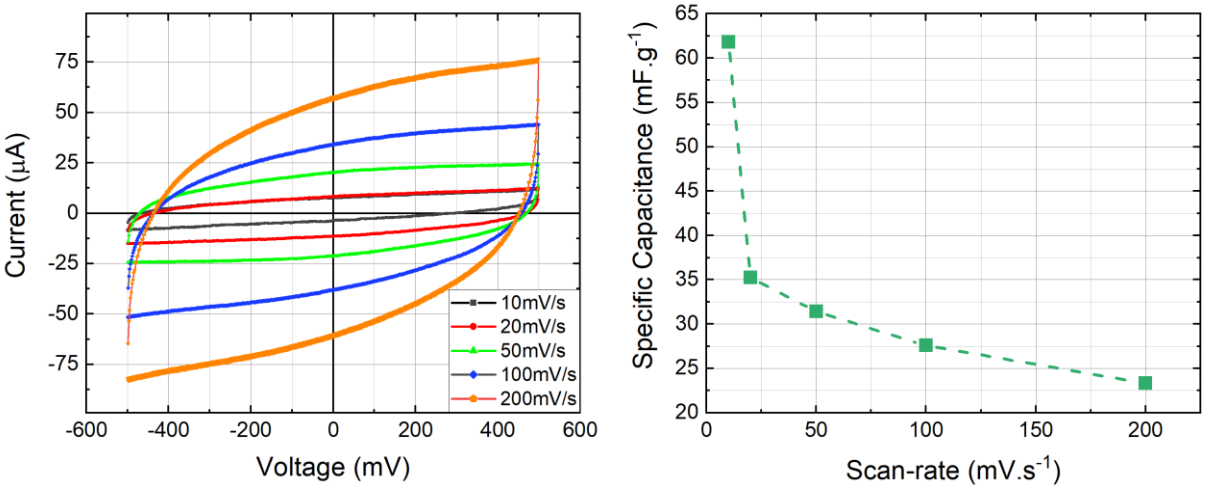

Figure 3.2 - Comparison between the performed Cyclic Voltammetry on the braid-like configuration without PPy with 9 turns **a)**. The tested scan rates of 10, 20, 50, 100 and 200mV/S with a voltage range of -0.5V to 0.5V are displayed. The obtained scan-rate vs specific capacity graphic **b)**.

Another studied variable that shown to have considerable impact on the device performance was the number of turns achieved on the braiding and twisting process, as described in reference [1]. To illustrate this, **Figure A. 1**, present in appendix A, shows the CV curves, followed by the SR vs SC relation, of a braid like device with 10 turns. Comparing the results of **Figure A. 1** with the ones present in **Figure 3.2** it is possible to verify that 10 turns capacitor archived increased capacitance values for the same scan rates and similar electrode mass. This indicates that more charge is being stored on the 10 turns device, as expected, due to its increase electrode active area, improving its specific capacitance

23% for the two lowest scan-rates and 32%, and 43% for 100 mV/s and 200 mV/s respectively. It is also noticeable an increased enhancement for the highest scan-rates. Furthermore, the attained CV results were acceptable, when compared with *Lima et al.* [1] performance for similar devices, the achieved SC shown to be lower for all tested SRs. Taking the example of 100 mV/s, the presented braid devices, with 9 and 10 turns reached a SC of 0.028 F. g^{-1} and 0.037 F. g^{-1} respectively, compared with the 0.09 F.g^{-1} presented in *Lima et al.* work [1]. The reason for these lays on the number of accomplished outer electrode turns around the inner electrode that, as described in the reference, greatly enhances the reached SC. Therefore, since the capacitors presented in the reference had 11 turns, the attained results from 9 turns and 10 turns braided devices shown to be very close, conferring additional mechanical stability to the capacitors.

The next study performed on non-functionalized braid-like configuration was CCD. For this, following the results from CV experiment, it was used a charge-discharge voltage from 0 V to 0.5 V, with 5 different charge-discharge currents (5 µA, 10 µA, 15 µA, 20 µA, and 25 µA). The results from this experiment are illustrated in **Figure 3.3** where it is visible the impact of the charge-discharge current on the device response time.

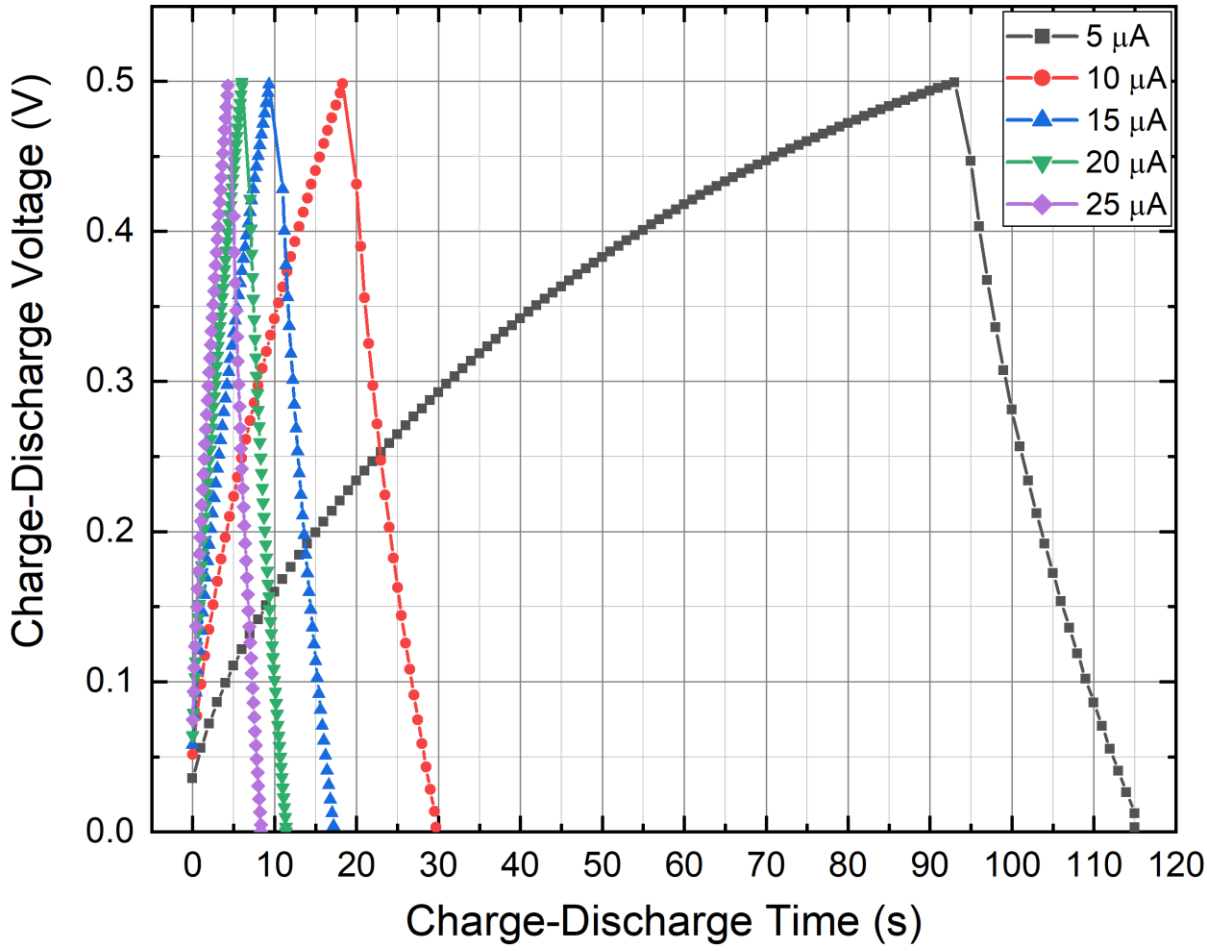

Figure 3.3 - Comparison between Charge-Discharge curves, with different currents, from the braid-like device without PPy and with 9 turns of the outer electrode onto the inner electrode. The tested Charge-Discharge currents displayed are 5 µA, 10 µA, 15 µA, 20 µA, and 25 µA and the curves correspond to the 9th cycle.

Moreover, the 10 cycles charge-discharge experiment, for each experimented current, were similar, showing the device performance stability on this cycle range. However, the first cycle tends to take more time than the following ones, especially for the lowest charge-discharge current. It was also visible a slight shortening in charge-discharge time from the 1st to the 10th cycle. This observation

suggests a slight loss in accumulated charge, within each CCD essay, that can be explained with electrolyte evaporation and consequent ion mobility loss, during the experiment.

3.2.2 Devices with PPy Coated Electrodes

Continuing the study of braid-like supercapacitors, the next step was to assemble new supercapacitors, adding the PPy coating process on the electrodes. For this enhanced version, 9 outer electrode turns were used to simplify the assemble process, and the same electric characterization methods were performed. However, CV essays were executed using scan rates of 50 mV/s, 100 mV/s, 200 mV/s and 400 mV/s and a voltage window from -1 V to 1 V. The sweep voltage window was increased, since PPy coated devices were able to maintain its quasi-rectangular CV curve with it. On the other hand, lower scan rates allow higher specific capacitance, however, these scan rates values were used to reduce the characterization experiments time, since, with the increased voltage window, it would be excessively time consuming. **Figure 3.4** shows the behavior of three braded devices, with 9 electrode turns each, for the different studied scan-rates. From this figure, it is possible to see that the three tested replicas shown similar behavior, presenting solid characteristic supercapacitor CV curves. Furthermore, within each tested scan-rate, the 3 braid-like replicas presented identical CV curves, which can be better observed in appendix **Figure A. 2**, solidifying the configuration reproducibility, despite its handmade nature.

Comparing the attained CV curves from the functionalized devices with non-factionalized ones, it is noticeable a great electrical performance enhancement with the functionalization step. This enhancement can be quantified though attained SC values, where is observed an increase of 1 order of magnitude as displayed in appendix **Table 1**. Moreover, the CV curves shape suffered a slight change on the voltage intervals of 0.8V to 1V and -0.8V to -1V, showing a pointy edge typical from pseudo capacitive device [41]. Additionally, using lower scan-rates on the functionalized device characterization would result in higher SC values, following the inversely proportional exponential behavior, displayed in SR vs SC graphic from **Figure 3.2** and **Figure 3.4**. Regarding the attained specific capacitances, **Figure 3.4** displays the SR vs SC relation for the three tested replicas. In this figure, it is again visible that, higher the scan-rate, lower the specific capacity resulting from the measurement, due to insufficient time for charges to accumulate. However, R3 shown a decrease in the specific capacitance for lower scan rates, visible comparing 100 mV/s and 50 mV/s results. This anomaly can represent a possible degradation of the PPy coating throughout the CV cycles allied with electrolyte evaporation. The effect of these phenomena is displayed in **Figure 3.5**, where the CV curve shrinks each cycle. On the right graphic of **Figure 3.5**, it is displayed the difference between the 2^{nd} cycle and 9^{th} cycle CV curve. Estimating R3 specific capacitance through the 2^{nd} cycle, it was obtained 0.39 F. g^{-1}, contrasting with the obtained 0.32 F. g^{-1} obtained through curve 9, approaching R3 results to R2 and R5 (presented in **Figure A. 3** in appendix A). Additionally, only 45 µL of electrolyte were added in the beginning of the complete CV measurement. Since the 50 mV/s scan rate was the last one measured of the four tested scan-rates, the impact of electrolyte evaporation is more evident on its results. Another possible contribution for R3 anomalous results can be related with the assembly process where, sometimes, broken carbon micro filaments, from the outer electrode, contact the inner electrode on its areas not covered by CA. As result, short-circuits between electrodes are formed, degrading the electric performance of the devices. This problem was spotted in other similar devices during CV measurement, deforming the attained CV curve. Yet, since the R3 CV curve, presented in **Figure 3.5**, did not suffer major visible changes, this scenario may not apply. Furthermore, the broken electrode filaments result in smaller usable electrodes area that reduces device performance.

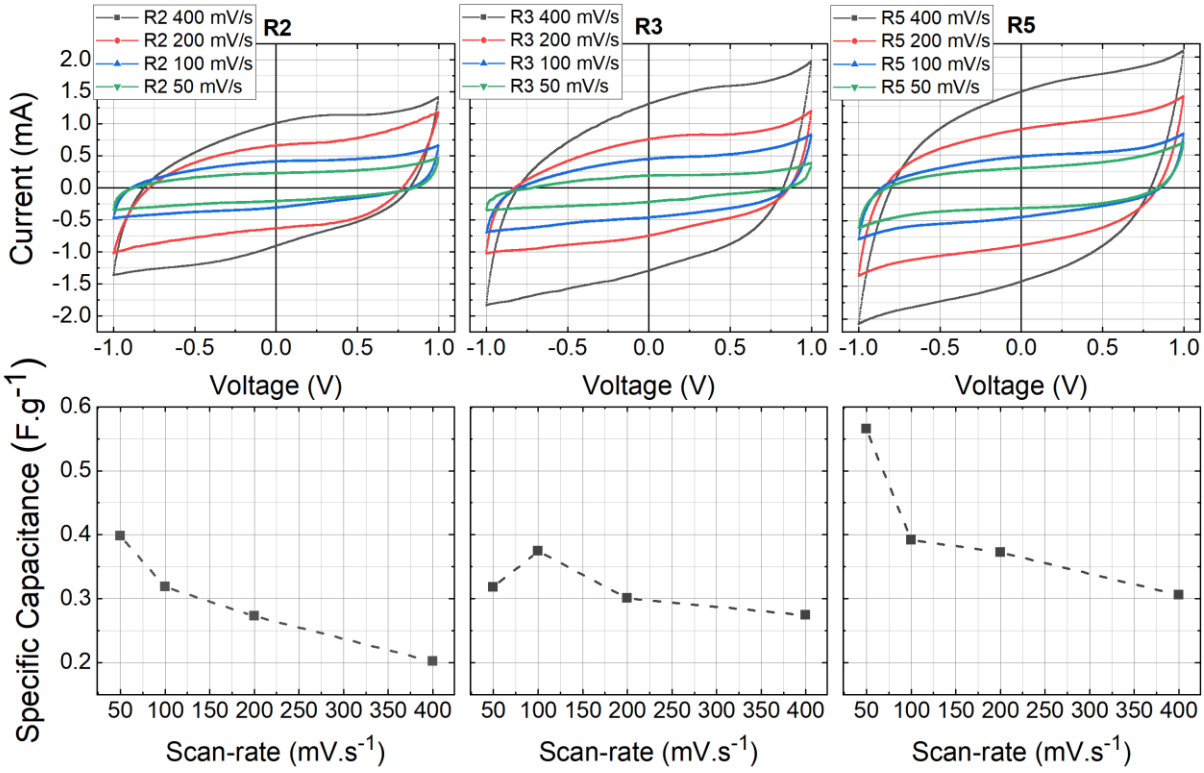

Figure 3.4 - Top: The obtain CV curves from the 3 braid-like functionalized replicas whit 50 mV/s, 100 mV/s, 200 mV/s and 400 mV/s scan-rates. **Bottom:** Display of the estimated SC with its correspondent SR.

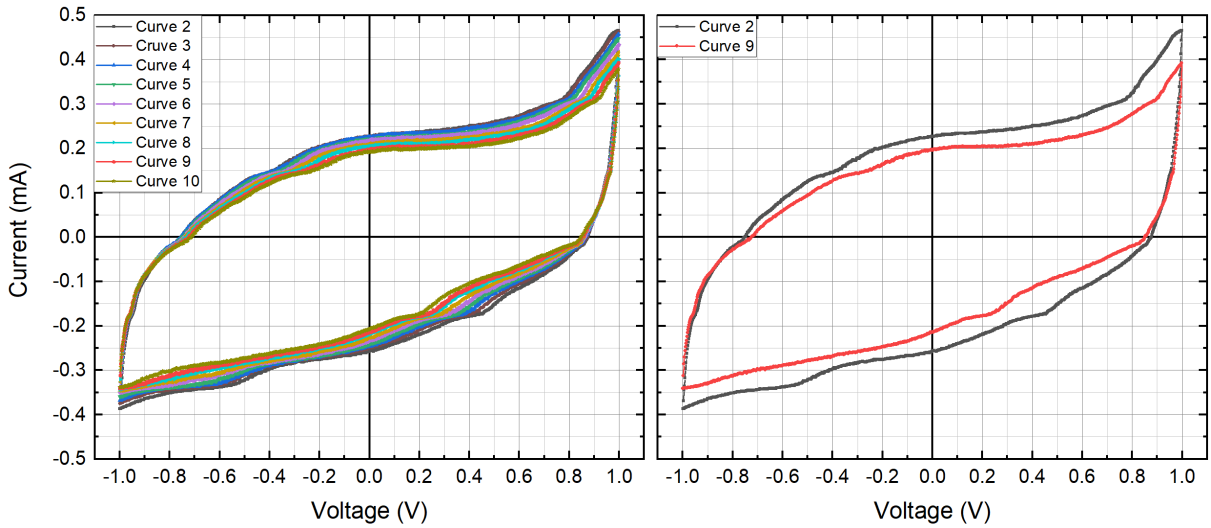

Figure 3.5 - Left: The effect of electrolyte evaporation during 10 cycles of CV measurement on R3 device, with 50 mV/s sane rate. **Right:** Difference between the 2nd cycle and the 9th cycle of R3 CV measurement, with 50 mV/s sane rate.

Henceforth, CCD essays were carried out to verify the device charge-discharge behavior. For this, 10 cycles of CCD were performed using 6 different charge-discharge currents, namely 50 µA, 75 µA, 100 µA, 150 µA, 200 µA, and 300 µA. The time normalized results are displayed in **Figure 3.6**, where it is visible that, higher the charge-discharge current, faster the process. However, R2 displayed a faster charge-discharge rate with 75 µA compared with 100 µA. This unexpected result can be related with the addition of electrolyte between experiments. The 10 cycle CCD essays were performed right after the 10 cycles CV runs, for each replica. Since the 1D supercapacitors suffer a rapid electrolyte

evaporation due to their low electrolyte volume, it was added 15 µL of electrolyte before starting the CCD experiments and in between the experiment for R2 and R3. This way the CCD study was started with the 100 µA charge-discharge run, followed by 150 µA, 200 µA and 300 µA. Then, 15 µL of electrolyte were added to perform the final experiment's that was the most time-consuming ones, respectively the 50 µA and 75 µA charge-discharge current. As seen in CV experiments, electrolyte concentration has a strong impact on device performance, thus, this experimental conditioning can be the reason for R2 unexpected behavior. Regarding R3, the influence of electrolyte addition is again visible despite the CCD curve with 100 µA be slightly faster than CCD curve with 75 µA. Respecting R5, its CCD performance shown to be within the expected since, contrary to R2 and R3, the electrolyte addition occurred only on the beginning of the CCD experiment and not within experiment.

Regarding device stability, within the 10 cycles CCD essays, the last charge-discharge cycles tend to be faster than the first ones, suggesting a loss in accumulated charge, over the cycle's progression. **Figure A. 4**, present in appendix A, illustrates this phenomenon, where the 2nd, the 5th, and the 9th cycles of 50 µA essay are compared. Coupled with the previous observation of electrolyte influence on the device performance, the shortening CCD curves throughout the cycles course, reinforces the braid-like devices susceptibility to electrolyte evaporation. A future study should be runed to reach configuration stability and define its electrical performance. Finally, it is visible a considerable discontinuity on the charge-discharge voltage, from the end of the charging cycle to the beginning of the discharging cycle. This phenomenon can be explained by the device electrodes internal resistance, that counteracts the charge flow during charge and discharge processes, resulting in the observed offset. Regarding the C vs SC results, the anomalous behavior of R2 and R3 are highlighted with the displayed deviation from the expected inversely proportional exponential behavior. Once more electrolyte concentration shown its decisive role on device performance. On the other hand, R5 performance was closer to the expected results.

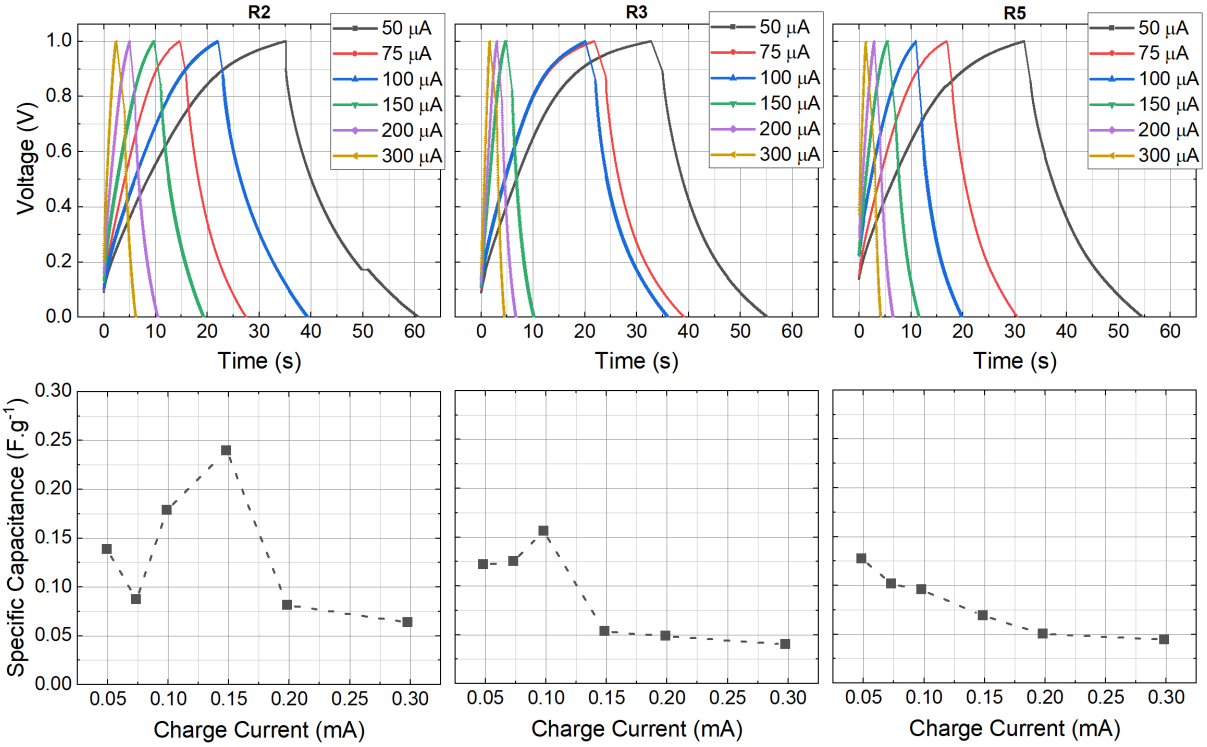

Figure 3.6 - **Top:** Comparison between the 9th cycle of each 6 different CCD charge-discharge current experiments, performed in R2 and R3. **Bottom:** Estimated specific capacitance vs charge current.

3.2.3 Washability study

One of the main novelties of this work is the device ability to work with its user's sweat. This characteristic adds biocompatibility and gives the device a remarkable ecofriendly nature, avoiding the use of strong acids, bases, and other aggressive electrolytes. Thus, the devices washability is a key characteristic to enable its application in reusable garments. To test the supercapacitor washing resistance, 5 washing cycles, followed by CV runs (using 100 mV/s scan-rate, with the previous sweep voltage window, from 1V to -1V, through 10 cycles) were carried out. An initial CV essay was performed before the first wash cycle to represent the standard supercapacitor behavior. Each washing cycle consisted of immersing the device in a 100 mL aqueous solution of current water and laundry soap (200 µL) and, leaving the device for 15 minutes under magnetic stirring (200 rpm), simulate a real washing cycle. Before every washing cycle, the supercapacitor was placed in a teabag to prevent its threads to get entangled around the magnet. To finish each washing cycle, the device was removed from the teabag, the remaining laundry soap was cleaned (with current water) and a drying process was carried out on a heating plate, at 40 ºC, for 20 min. Finally, the CV measurement were performed. The results, from the 5 washing cycles, performed in R0 and R2, can be seen in **Figure 3.7**. It is noticeable the higher variability of R0 in respect to R2, between each washing cycle. Moreover, R0 had been previously used for CV testing, as previously referred, which possibly caused some damage on the electrodes PPy coating. This assumption is supported by the attained results, sown in **Figure A. 5** on appendix A, where it is visible an anomalous behavior on its CV assay. On the other hand, ignoring the results from cycle 3 and 4, R0 washing study conclusions resemble the ones from R2, since both devices shown the ability to maintain most of their CV curve shape, throughout the washing cycles. However, R0 results cannot be considered a very accurate representation of the braid-like devices behavior. Regarding R2 results, even though its CV curves shape are mostly maintained, it is noticeable a slight decrease from cycle to cycle, suggesting a continues loss of PPy coating from its electrodes. Particularly from the outer electrode, as it is the one without any covering layer.

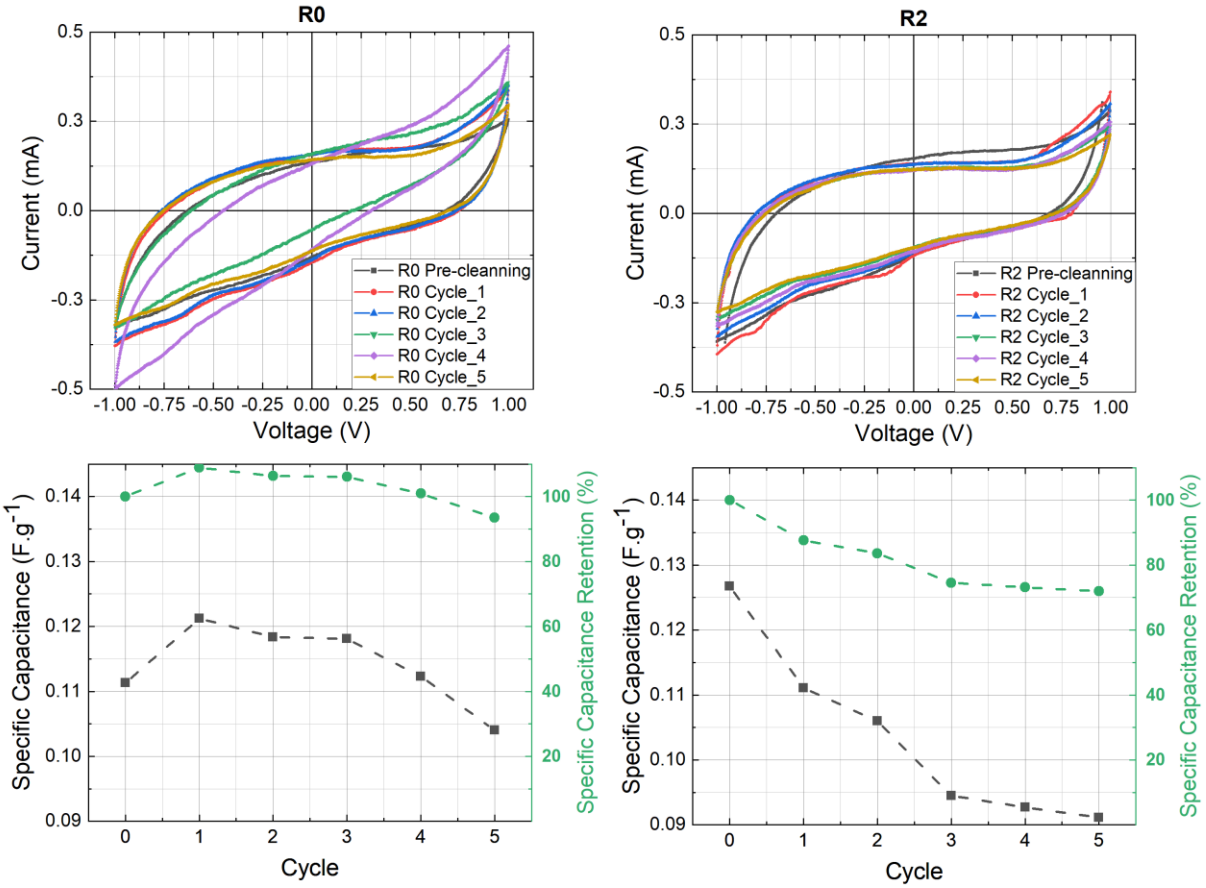

Figure 3.7 - CV curves obtained with two lD braid-like devices, before starting the washing experiment, and after every washing cycle, for a total of 5 cycles. The CV parameters used were 100 mV/s scan-rate and sweep voltage window from -1 V to 1 V. In this figure it is displayed the 9th cycle of each CV experiments performed.

Furthermore, for both devices, **Figure 3.7** shows a different path when traveling from negative voltage to positive voltage and in the opposite direction. This fact suggests an unevenness on the electrode's electrical performance. Moreover, the path difference is already present on the pre-washing cycle, and the pre-washing results differ from R2 CV curves, previously measured, displayed in **Figure 3.4**. This observation may imply a previously delt damage on the outer electrode coating, probably caused by scraping the device while handling and/or storing it, before performing the washability study. Adding to this possibility, the device was rolled in lab paper to be stored, and some excessive friction may have caused the PPy coating to peel of form the outer electrode. Consequently, even though R0 and R2 shown to maintain their CV curves shape throughout the washing experiment, it is possible that the PPy, from the functionalized outer electrode, had been peeled of, before the experiment. Finally, although the promising results displayed in **Figure 3.7**, to reinforce the discussed conclusion of braid-like device ability to maintain its electrical performance after wash, the experiment should be repeated with new replicas.

3.2.4 Cyclic charge-discharge endurance for 1000 cycles

Supercapacitors cyclic stability was also studied once it represents a key characteristic for the device success on reusable applications. Therefore, it was performed a 1000 cyclic charge-discharge test to analyze the supercapacitor performance and stability. However, no countermeasures were considered to prevent electrolyte evaporation, and its impact is very noticeable on the braid-like replicas CCD performance, as displayed in **Figure 3.8**. It was observed an SC decrease of 75.4% and 75.5% from the 5th cycle to the 105th cycle, to R1 and R5 respectively. This represents a major performance degradation on the first 100 cycles (considering the 5th cycle the beginning cycle) due to the electrolyte evaporation. Moreover, the replicas R1 and R5 respectively loss 16.9% and 15.9% of SC, from the 105th

cycle to the 1000th cycle, suggesting that most of the electrolyte evaporate during the first 100 cycles. Appendix **Figure A. 6** displays the attained CCD results, from cycle 5 to cycle 905 with a 100 cycles step and ending on the 1000th cycle, as displayed in **Figure 3.8**, and an additional close up from 205th cycle to 1000th cycle to better visualize the replicas CCD performance. It should be noted that, for real life application electrolyte would have periodic additions from its user sweat and the device performance should not degrade so fast.

Additionally, comparing the first 10 cycles of the 1000 cycles CCD results, with the previous 10 cycles CCD study, with 100 µA charge-discharge current for the 2 braid-like replicas, it is noticeable a discrepancy on the charge-discharge time. Moreover, the conditions for both studies were similar, which should result in similar results. Since devices R2 and R3 had already been used to perform the CV experiment, before the 10 cycle CCD test, their shorter charge-discharge times, using the same 100 µA, can be related with some degradation during the CV essays. Therefore, future studies should be carried out to better characterize and describe a more suitable device operation range. Furthermore, this result can also indicate a discrepancy on device replicas mostly due to the device assembly process.

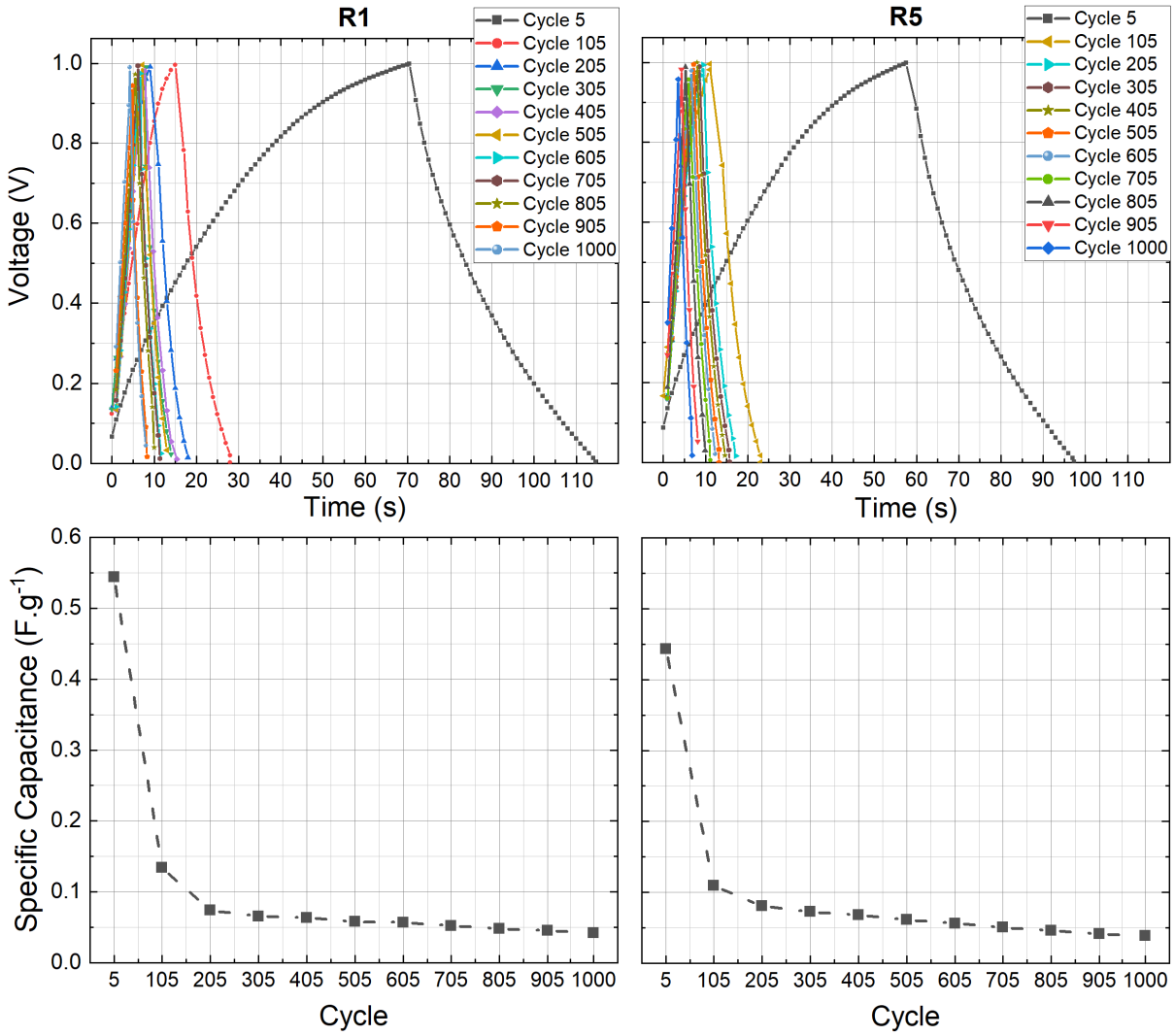

Figure 3.8 - **Top:** Results of the 1000 cycles CCD performed on 2 braid-like replicas, from cycle 5 to cycle 905 with a 100-cycle step and ending on the 1000 cycle. **Bottom:** The correspondent SC estimated for each cycle.

3.3 Woven configurations

Following the lines of Braid-like configuration chapter, this section will be regarding the results obtained with the study of the archived woven configurations. Initially, carbon yarns and fabric devices will be experimented. Then, PPy electrodes functionalization will be added and studied as in the previous chapter.

3.3.1 Without PPy coated electrodes

The first woven configuration approached was the parallel external electrodes structure, constituted by two carbon threads (electrodes) woven in a hydrophilic felt fabric. The first study carried out for these devices was the electrodes distance influence on its electrical performance. To accomplish this, parallel woven devise, with electrodes distance of 0.1 cm ,0.3 cm, 0.5 cm and 1 cm (as displayed in **Figure B. 2**) were assembled and tested. Moreover, the piece of felt measured around 1.5 cm x 4 cm and the effective woven electrodes length was 3 cm. The electrical experiment performed for this comparison was CV since it reveals the supercapacitor electrical behavior. As the first stage of braid-like device testing, it was used scan rates of 10 mV/s, 20 mV/s, 50 mV/s, 100 mV/s and 200 mV/s with -0.5 V to 0.5 V voltage window. These preliminary experiments were carried out using half yarn for the electrodes with the objective to minimize the used electrodes material and improve the carbon yarn's ability to be woven. Whoever, these devices shown to be very difficult to handle due to the carbon yarns structural stiffness, allied with the brittle nature of the constituting carbon microfilaments. Consequently, some carbon filaments broke during the woven process due to the resulting tangential strain, leading to the formation of short circuits between electrodes. As result, the electrical performance of the device was strongly degraded, making them unfeasible. Therefore, the electrical measurements were repeated, using devices with complete carbon yarns as electrodes. Although the fragile nature of the carbon threads still led to occasional short circuit, the devices handling was significantly improved. Moreover, electrode distance of 0.1cm proved to be small for the yarn's brittle nature, even using full yarn electrodes. **Figure 3.9** illustrate the difference between half and full electrode devices. In this figure it is visible that, for the lowest and highest CV scan-rates, full electrodes devices can store more charge due to their wider surface area. For the lowest scan-rate, the CV curve presents a rough aspect and is shifted to the negative part of the current axis. The first condition relates with the low scan-rate used to perform the experiment, resulting in currents close to the potentiostat definition limit. The second is related with an unevenness on the electros size and possible damaged filaments that result in a difference between electrodes resistance and surface area. Another variable that can influence the current axis shift is the electrolyte distribution around the electrodes. When it is not even for both electrodes, the electrode/electrolyte surface will differ, resulting in a mismatched charge accumulation between electrodes.

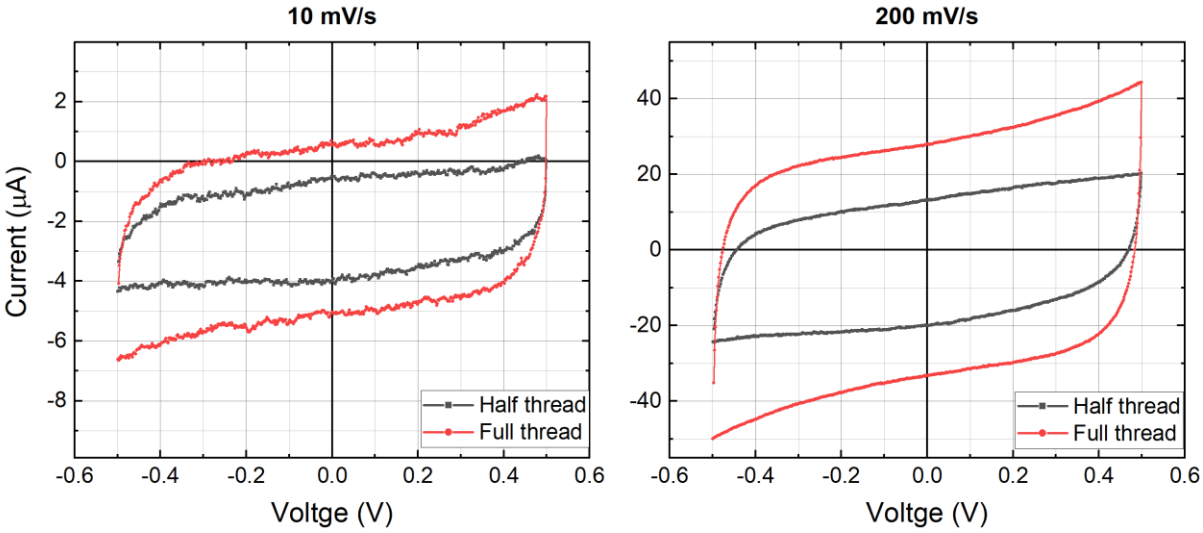

Figure 3.9 - CV graphics performed with the 0.3 cm electrodes paralleled woven device to illustrate the difference between the obtained results with full and half thread electrodes.

Regarding the electrode's configuration, it was initially experimented the half thread parallel and crossed configuration with external electrodes. Crossed configuration presented additional trouble for the referred short-circuit formation. Because of this, only devices whit electrodes distance of 0.5 cm and 1 cm were possible to test. Additionally, comparing the resulting CV curves from crossed and paralleled half electrodes configurations, parallel configuration shown similar results or even better in some cases. **Figure 3.10** illustrates the comparison between the parallel and cross configuration with half yarn electrode. Because of this, the parallel configuration was used to carry on the CV experiments with the full yarn electrodes.

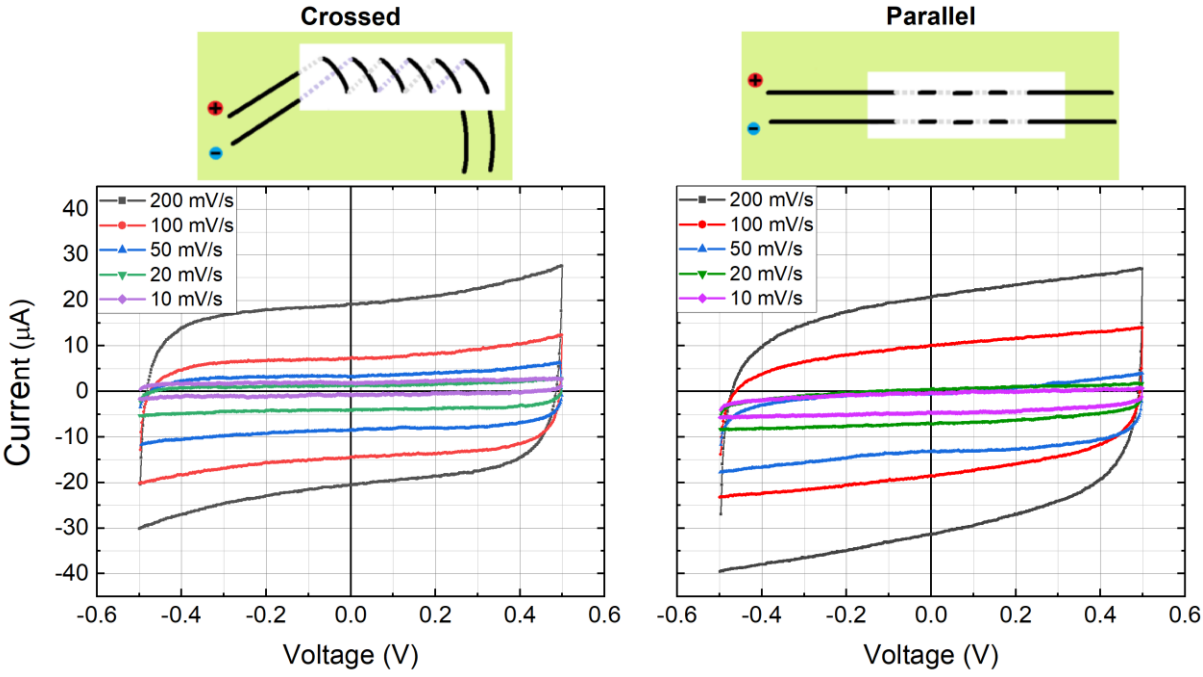

Figure 3.10 - All scan-rates CV results from crossed and parallel woven devices, with 0.5 cm of electrodes distance.

To further improve the short-circuit resistance of parallel full thread electrode supercapacitor, the parallel internal configuration was assembled and studied. The idea was to pass the thread electrodes inside the felt fabric, using it as a barrier to better protect and insulate the electrodes from each other, as displayed in **Figure 2.1**. Hence, the felt dimensions were changed for 1.5 cm x 3 cm to achieve a similar active electrode length for both configurations. With this new approach, the short-circuit was successfully reduced, although it continued happening for the 0.3 cm, and the 0.1 cm electrode distance was still not manageable. Contrasting the two configurations CV results, the internal configuration presents wider CV curves (as displayed in **Figure 3.11**), indicating more charge accumulation. This slight enhancement relates with the wider electrode/electrolyte contact surface, promoted by the electrode's arrangement since the internal configuration allows a wither active electrodes area, maintain the same woven electrode mass. Comparing the estimated specific capacitance, from both configurations, the enhanced ability of the internal device to accumulate charge is confirmed, as displayed in **Figure 3.12**. This enhancement was observed for 0.5 cm and 1 cm electrodes distance as well. Furthermore, due to its simplicity, higher specific capacitance, and more robust structure, the internal configuration with full thread electrode was used to continue the study of the woven supercapacitors with functionalized electrodes, that will be further discussed.

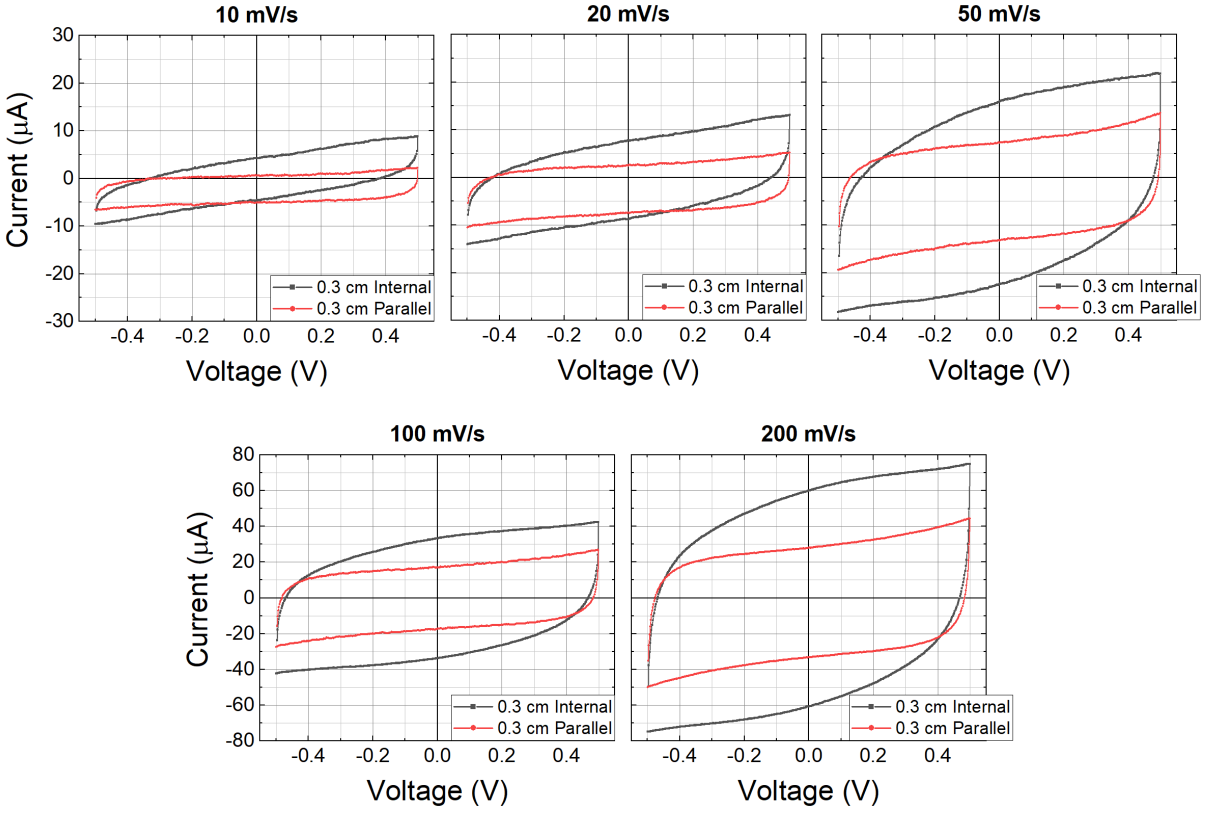

Figure 3.11 - Graphic illustration of the CV curves (9th curve of the 10 cycle CV experiment with each scan-rate) resulting from parallel and internal woven configuration, both with full electrodes.

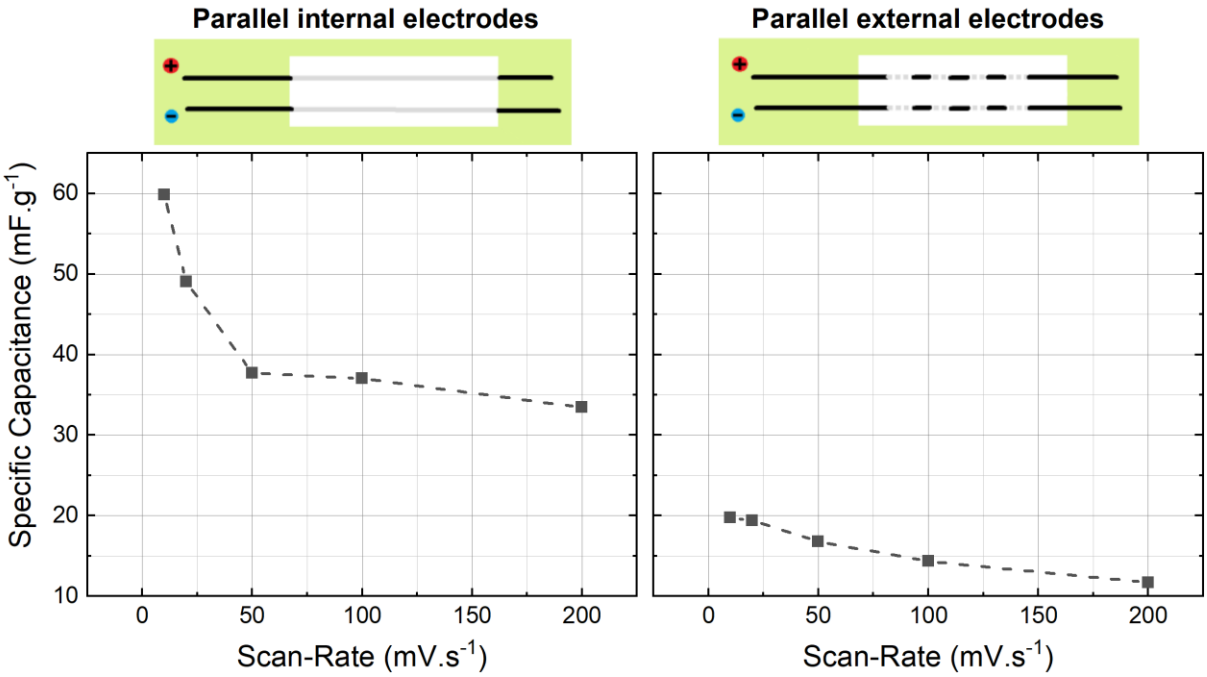

Figure 3.12 - Graphic representation of the attained SR vs SC, from the woven configuration featuring parallel external electrodes (right) and internal electrodes (left) with 0.3 cm of electrodes distance.

After the arrangement study, electrode distance analysis was carried out to understand its influence on the device specific capacitance. With this intent, a CV experiment was carried out on devices with 0.3 cm, 0.5 cm, and 1 cm electrode distance, as displayed in **Figure 3.13**. Note that, in the figure, it is missing the CV curves with 10 mV/s and 20 mV/s from 1 cm electrodes distance device. Unfortunately, the lack of this measurements was noticed late in the data analysis making unfeasible their performance. Observing the top left graphic of electrodes distance vs specific capacitance, it is visible that, for the lowest scan-rates used, the attained SC is higher for 0.5 cm instead of 0.3 cm electrodes distance. This result does not follow **Equation 1.2** in the Introduction chapter, which describes an increase in the device capacitance with electrodes distance decrease, maintaining the remaining variables constant. A potential cause for the observed behavior can be related with the unprecise electrodes handmade sawing process, allied with the device sensibility to small electrodes movements during device handling. This way, since the 2 mm difference from 0.3 cm and 0.5 cm devices is not precise, and the electrodes can be moved inside the felt easily, the 0.5 cm device can have its electrodes closer than the 0.3 cm device. Broken carbon filaments, associated with the woven process, can also explain the observed result if hypothetically, the 0.3 cm device had more broken filaments than the 0.5 cm device, reducing its electrodes usable area [33]. The fact that this anomalous behavior is observed only for lower SR, where the electrolyte ions have more time to organize tighter around the electrodes [41], contributes to the broken filament's hypothesis. On the other hand, closer the electrodes, higher the risk of short circuit formation duo to broken filaments, as described before. The short circuit influence was observed on the parallel configuration with full and half thread electrodes, usually resulting in a total malfunctioning device. Furthermore, this study illustrated the need to find a balanced electrodes distance, able to avoid short circuit formation while maintaining the best electrical behavior possible. Regarding the 1 cm electrodes distance, although functional, resulted in lower SC values, as expected.

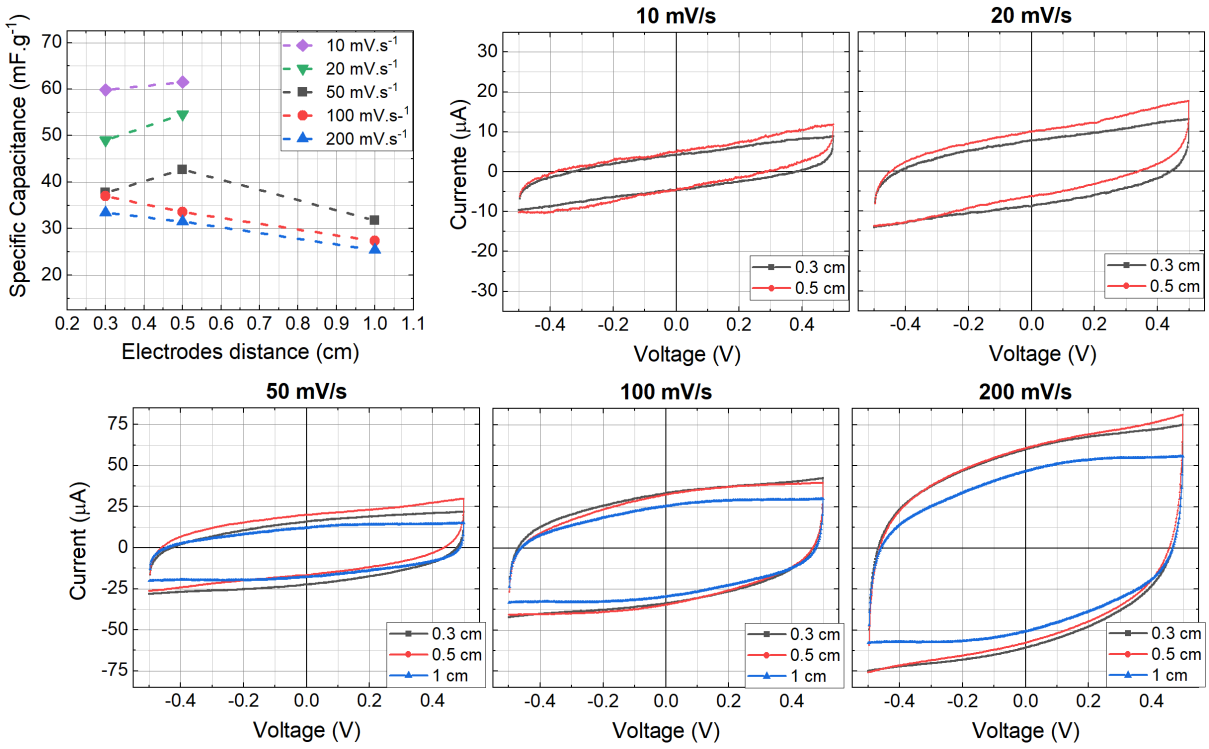

Figure 3.13 - Top left: Graphic representation of SC vs electrodes distance, measured on the internal woven configuration. **Remaining:** Graphic representation of the attained CV curves from the different experimented electrodes distance on the internal woven configuration.

Continuing the study of woven devices with standard electrode, CCD assays were performed on the internal and external configuration to illustrate its charge-discharge response. Crossed configuration was not included in CCD assays due to its short circuit condition. The focus of this step was to verify the CCD stability, as well as the influence of the charge-discharge current. For such, only devices with 0.3 cm and 0.5 cm electrode distance were tested, since these distances presented the better results on the CV experiments. **Figure 3.14** displays the CCD results, obtained for 5 different charge-discharge currents, applied on the internal configuration with 0.5 cm electrodes distance and the external arrangement with 0.3 cm electrode distance. As expected, CCD assays with low charge-discharge currents result in higher charge-discharge times. Regarding CCD curve shape, they present supercapacitor characteristic, reenforcing the double layer mechanism [1], [41]. Moreover, even though there is no rest time between charge and discharge cycles, it is noticeable that all CCD curves presented a discontinuity between charge cycle end and discharge cycle beginning. This suggests that the teste woven devices instantly discharge a small percentage, being unable to hold its full charge, which indicating that the 0.5 V charge widow is high for preliminary devices. Since this was still a preliminary experiment with an illustrative objective, 1 cm devices were not addressed.

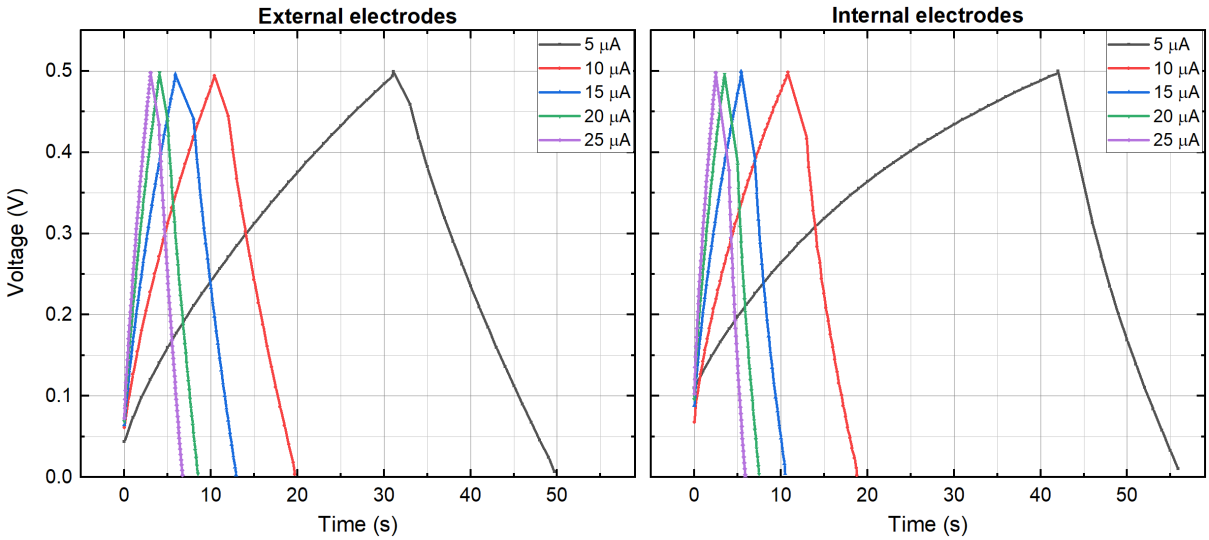

Figure 3.14 - CCD results from woven parallel configuration with internal (right) and external (left) full electrodes. The electrodes distance are 0.3 cm and 0.5 cm, respectively and it is displayed the 9th cycle of each CCD assay.

Furthermore, **Figure 3.15** presents the CCD results from 0.3 cm and 0.5 cm, within internal and external electrodes disposition. Note that the lowest testing charge-discharge currents differ from 5 µA, on the external configuration, to 10 µA on the internal configuration. This happened because the 5 µA current was only used on the internal device with 0.3 cm electrode distance, with the objective to saving time, and the CCD measurement whit 10 µA was not performed on the external devices with 0.3 cm electrodes distance by mistake. Although, the presented results are suitable for the illustrative purpose of these preliminary experiments. Herewith, **Figure 3.15** shows that, within the same configuration, internal electrode devices shown a decrease in charge-discharge time with the increase of electrode distance, for the same charge-discharge currents. However, external electrode configuration only shows the same behavior for the lowest tested charge-discharge current. This peculiar behavior can be related with the extra 10 µA CCD run performed on the external electrode device with 0.3 cm electrode distance. This extra measurement, with a low charge-discharge current, induced more time for electrolyte evaporation. Thus, since the CCD measurements were performed following the ascending order of charge-discharge current, the CCD measurements with 15 µA, 20 µA, and 25 µA, were carried out in different electrolyte evaporation conditions, between 0.3 cm and 0.5 cm electrode distance devices. Hence, it was shown once more the electrolyte evaporation susceptibility of the presented devices. Regarding the comparison between the internal and external electrode arrangement, the internal electrode devices shown to have faster charge-discharge cycles for the same currents. Once more, this is not observed when comparing the 0.3 cm internal and external electrode capacitors because the extra electrolyte evaporation on the external electrode device. Moreover, concerning the cyclic stability, all 10 runs, within the same charge-discharge current experiment, presented similar curves evidencing the device stability. Additionally, new measurements with equal conditions should be carried out to solidify the presented results.

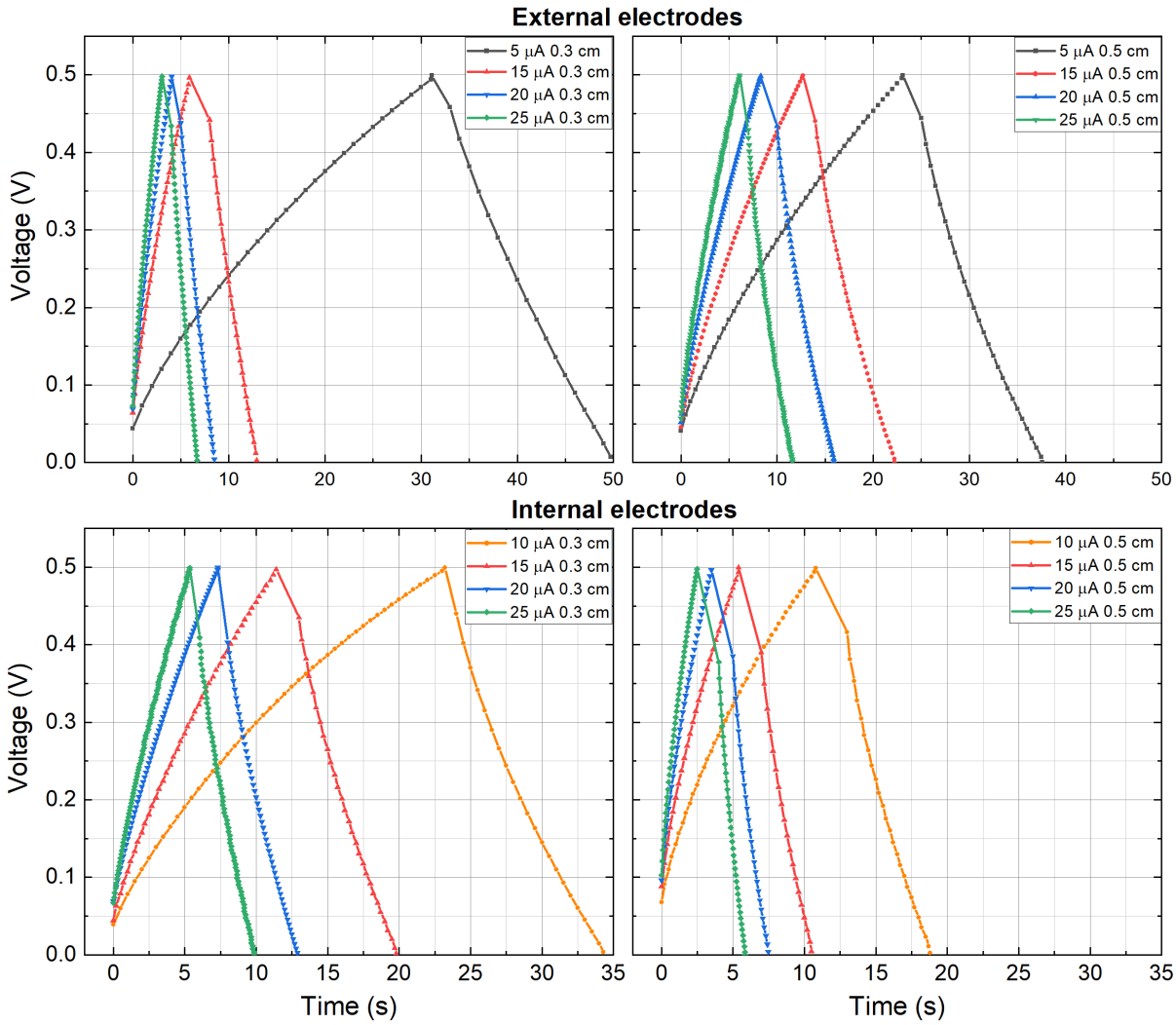

Figure 3.15 - **Top** - CCD results from woven parallel configuration with external electrodes, 0.3 cm (left) and 0.5 cm (right) apart. **Bottom** - CCD results from woven parallel configuration with internal electrodes, 0.3 cm (left) and 0.5 cm (right) apart. The present curves were obtained from the 9th cycle of each experiment.

3.3.2 Four threads woven device

To explore the interaction of multiple capacitors woven in the same piece of felt, four thread devices were assembled and experimented. For this study, pieces of felt with the same dimensions practiced for the internal electrode configuration, were woven, using only carbon electrodes, with 0.3 cm between them. Moreover, parallel and series electrode configurations were assembled and tested, as displayed in **Figure B. 3**. The CV experiment was performed following the 10 cycles for each tested SR, as before, however, it was used the SR of 50 mV/s, 100 mV/s, 200 mV/s, and 400 mV/s, speeding up the experiment and adding the 400 mV/s measurement to this carbon only electrode configurations. The results are present in **Figure 3.16**, showing once again, the device EDL nature and stability for the 10 cycles within each tested SR. Furthermore, the parallel arrangement reached about the double of the SC, when compared with the single internal woven device, following the behavior of capacitors connected in parallel. Likewise, although not accurate with the expected theoretical behavior, the series arrangement shown a specific capacitance slightly lower than what was obtained with the single capacitor experiment, following the behavior of capacitors connected in series [33]. This departure from the expected behavior can be related to the electrolyte share between devices, which can be contributing to a closer single device behavior. Moreover, since the voltage drop is divided by the capacitor, when connected in series, higher voltage inputs can be applied. This phenomenon is illustrated in appendix **Figure A. 7**, where a voltage window from -1V to 1V was used for the CV runs. In particular, lower SR

resulted in better CV curves for these runs. Additionally, the CV and CCD results attained with the second parallel configuration tested where similar to the first one, with the exception of charge-discharge time that shown to be longer for higher charge discharge currents on the second configuration. The respective results can be seen in appendix **Figure A. 8**. In sum, the four threaded device experiments illustrate the carbon only device ability to be arranged in a multi-electrode way, allowing to modulate and reach higher device specifications in a single piece of garment.

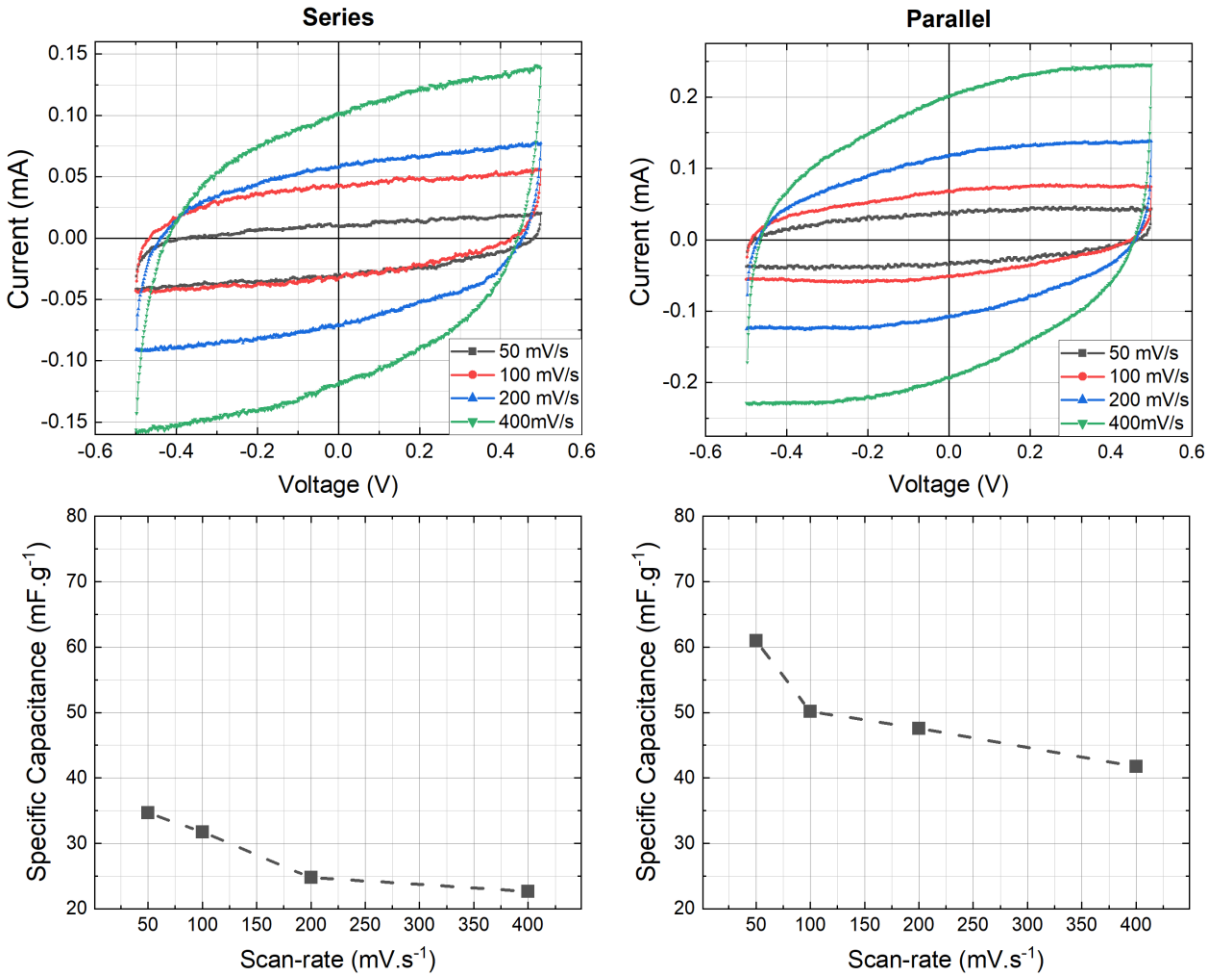

Figure 3.16 - CV results attained with internally woven internal electrodes capacitors, connected in series (left) and in parallel (right).

3.3.3 With PPy coated electrodes

Based on the obtained results from the preliminary woven device, the study was carried out on supercapacitors with functionalized electrodes, for the internal configuration. Despite electrodes distance of 0.5 cm shown better results on preventing short circuit formation and, electrodes distance of 0.3 cm and 0.5 cm presented similar CV results, it was used the 0.3 cm to advance for the functionalized electrodes study. The reason for this is based on the theoretical fact that, closer the electrodes, higher the accumulated charge. Following the steps of braid-like device study, three similar replicas of factionalized woven internal electrodes supercapacitors, with 0.3 cm electrodes distance, were assembled and tested to verify their performance and reproducibility. Once more, CV (with voltage -1 V to 1 V voltage window and scan rates of 50 mV/s 100 mV/s 200 mV/s and 400 mV/s) and CCD (with 50 µA, 75 µA, 100 µA, 150 µA, 200 µA, and 300 µA charge-discharge current) experiments were conducted. As seen in the braid-like study and reference [1], **Figure 3.17** shows that PPy electrodes functionalization greatly enhances the charge accumulation for the woven supercapacitors, as well.

Furthermore, comparing the CV results from the 3 replicas, it is visible the variability between them, better displayed in **Figure A. 9** on the Appendix section. This variability can be justified with the devices sensibility to the assemble process, especially during the woven step, where the PPy coating can be slightly striped off from the electrodes. Moreover, the electrodes functionalization step also adds device performance variability through inconsistent coating uniformity and thickness, which may also lead to unevenness between electrodes. In addition, PPy coating impact is noticeable when comparing the CV curves obtained for R3 with the ones displayed by the R1 and R2. Once PPy is reported to add pseudocapacitive behavior to supercapacitors [14], [15], and R3 CV curve shape present pseudocapacitive traces [41], with wider CV response, it is possible to conclude that R3 results are related with a better PPy electrode coating.

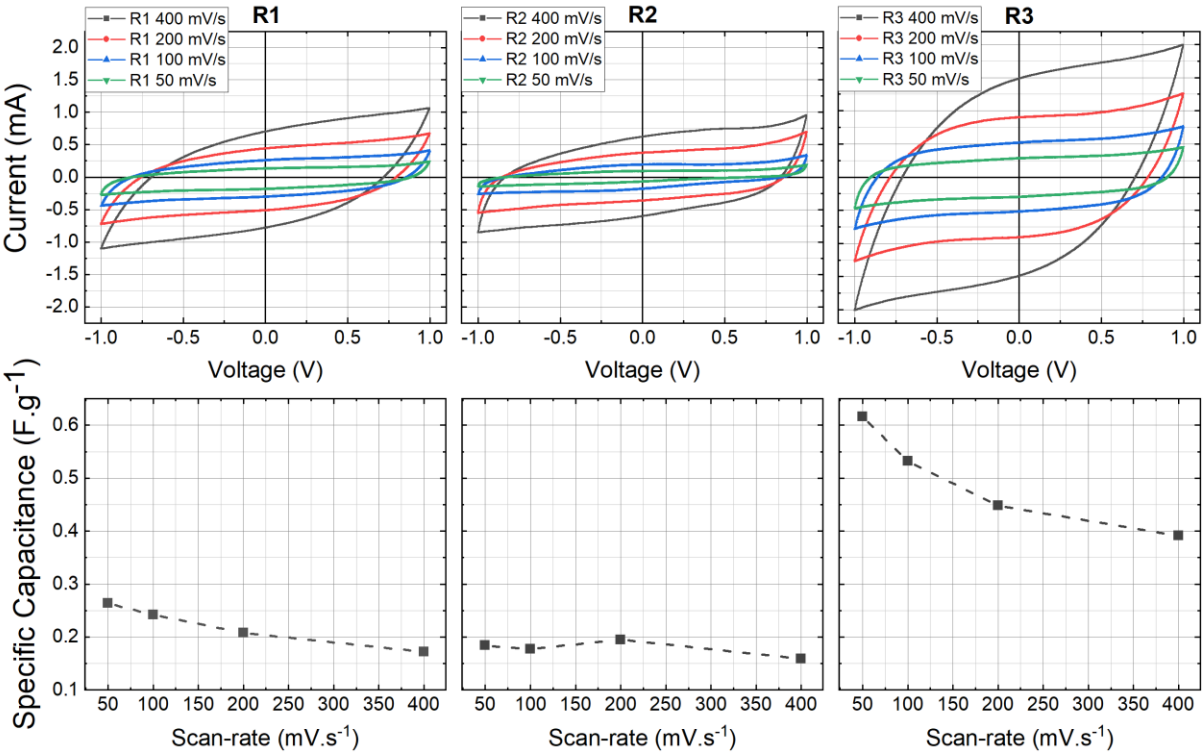

Figure 3.17 - CV results from three similar internally woven devices with PPy functionalized electrodes, 0.3 cm apart, followed by the estimated specific capacitance values vs scan-rate.

In terms of SC vs SR values, R3 shown considerable better performance than R1 and R2 as anticipated from its CV curves shape. Regarding R1 and R2, they have shown similar results, however, R2 exhibit an unusual behavior, since the highest SC achieved was with 200 mV/s SR. This unexpected behavior can be justified with slight PPy detachment during CV measurements, showing the electrode coating susceptibility for this event. Additionally, R3 performance is comparable with functionalized braid-like devices, showing even higher values, which is remarkable considering its electrodes distance (being both devices with similar functionalized electrodes size). The use of all electrodes surface area, on the internally woven electrodes devices, allied with a more successful sewing process and more uniform PPy coating, can explain R3 considerable performance. This way, although replicas R1 and R2 presented similar results, R3 illustrates the device potential with a more controlled manufacturing process.

Regarding CCD assays, through **Figure 3.18**, it is visible a considerable variability between the replica's electrical behavior, following the observations on CV experiments. This result suggests an irreproducible manufacturing process, with possible causes being the inconsistency of PPy electrodes coating and its peel-off during the woven process. Once more, the need for a better studied and controlled manufacturing process, shown to be mandatory for functionalized woven devices success, as

verified with R3 performance. Furthermore, comparing the results within each CCD experiment, it is visible a slight decrease in charge discharge time through each cycle, as illustrated in **Figure A. 10**. This observation is more evident for CCD experiments with the lower charge discharge currents, once, for these currents, there is more time for electrode/electrolyte ion transfer mechanics to take place, enabling the device to reach higher charge density for these CCD cycles [41]. Thusly, any change on the active components of the supercapacitor is more evidenced. For these devices, although electrolyte evaporation still has its role, it does not seem to justify the observed CCD performance variation, once the hydrophilic felt maintains the electrolyte adsorbed to its fibers for a longer period. Consequently, the charge-discharge time decrease throughout cycles, can be related with a slight coating degradation on the electrodes, which will be more discussed in *Cyclic charge-discharge for 1000 cycles* in woven devices sub-chapter. Notwithstanding, the relation between charge discharge time and respective current is coherent for the 3 replicas, with R2 showing the shortest curves, due to the PPy detachment discussed above.

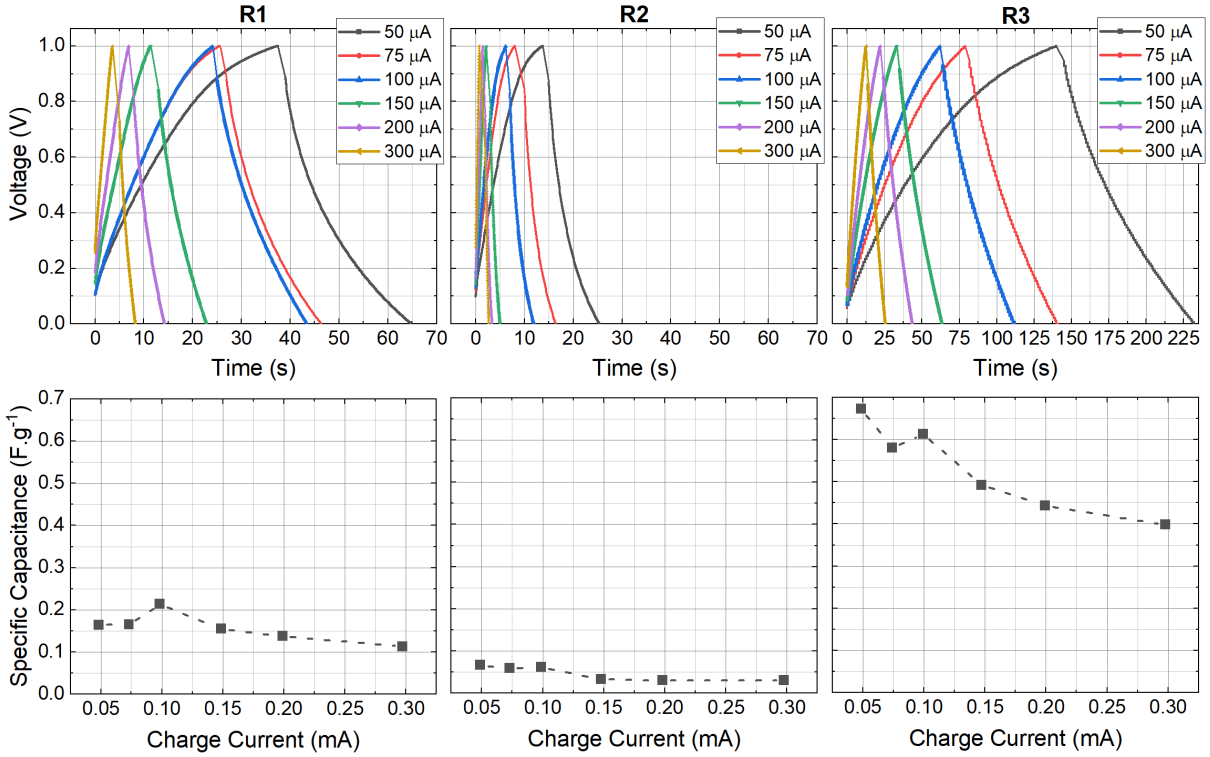

Figure 3.18 – **Top:** Graphic results from 10 cycle CCD experiment with six different charge-discharge currents for the three functionalized internally woven replicas. **Bottom:** Respective specific capacitance vs charge current relation for each replica.

3.3.4 Washability study

As executed in braid-like devices, the next step on functionalized woven supercapacitors was to investigate the influence of washing cycles on their electrical performance. Once more, two devices (R0 and R3) were submitted to 5 washing cycles of 15 minute, following the described protocol in braid-like configuration, *washability study* sub subject. The only exception was the drying time before washing that had to be extended for 1h due to the hydrologic felt nature and its bigger area to adsorb water. **Figure 3.19** displays the comparison between each device CV performance, before washing and after every washing cycle. Specific capacitance results show that the 2 tested devices were able to maintain most of their original performance through the 5 cycles. It is noticeable some oscillation on SC values since the devices seem to recover their performance on cycle 5 and 4 for R0 and R3 respectively. However, this phenomenon can be attributed to the associated experimental error, allied with little electrode movement during washing cycles, which results in a slight variation on electrode

active area. Moreover, comparing the pre-washing CV data of R3 with it previous CV experiment in the same conditions, performance degradation is visible, suffering a SC decrease of approximately 0.1 F.g $^{-1}$ (around 18% performance loss). Once more, PPy coating degradation is suggested as the cause for such loss.

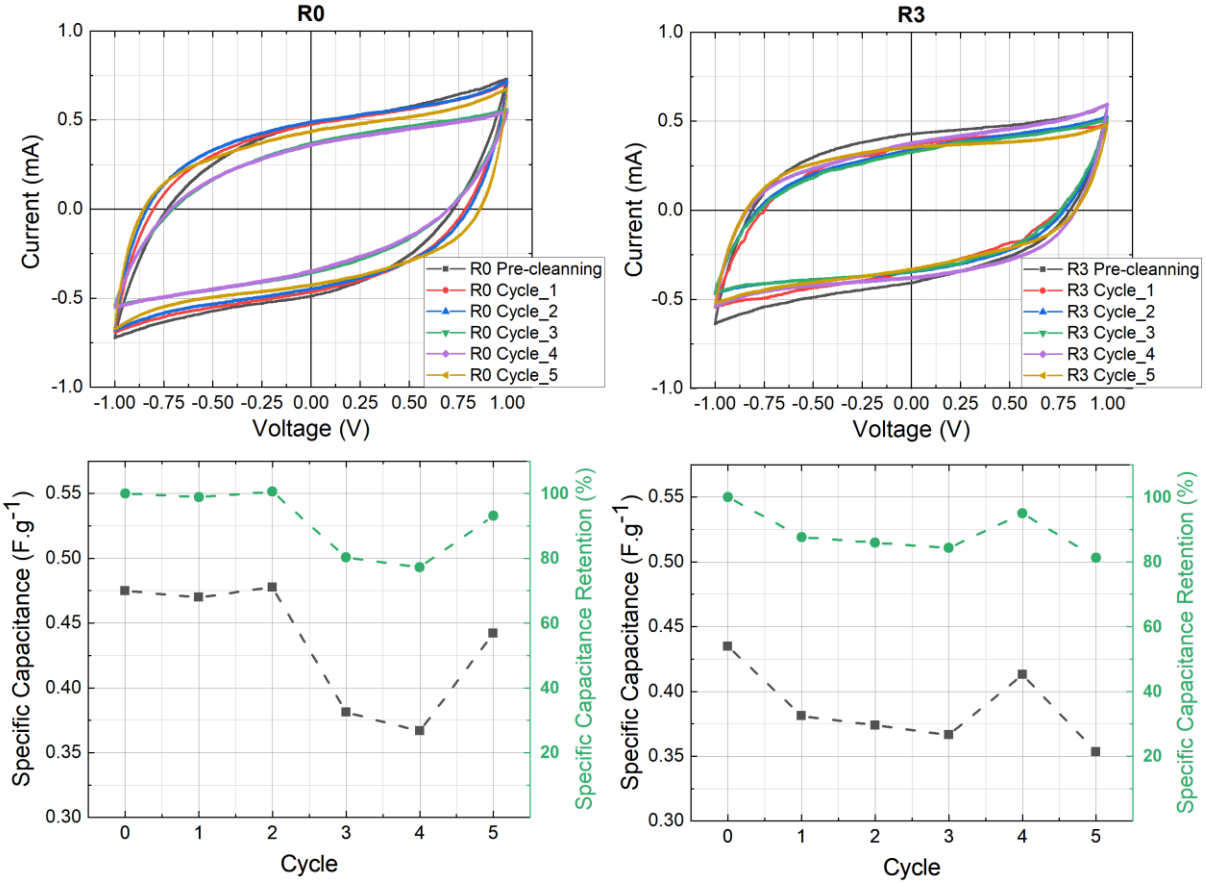

Figure 3.19 - CV results (with 100 mV/s SR) from woven devices washing experiment. It is presented the 9th CV curve of 10 that composed each experiment.

Moreover, it was not observed significant differences within most of the 10 CV cycles for each experiment. However, slight electrodes adjustments were needed, after some watching cycles, in other to get the expected CV curves. Otherwise, CV curves world present random shapes and deformations, caused by the formation of electrode bridges through detached PPy clusters or broken carbon filament, present on the felt/electrode interface. Nevertheless, woven supercapacitors shown themselves washable.

3.3.5 Cyclic charge-discharge endurance for 1000 cycles

To finalize internally woven electrodes device study, it was performed the 1000 cycle charge-discharge endurance experiment on 2 supercapacitors (R1 and R2). Once more, device performance degradation was visible throughout the experiment, as displayed in **Figure 3.20** and appendix **Figure A. 11** where is displayed the device CCD curves form cycle 5 to cycle 905 with a step of 100 cycles in between and ending on the 1000 cycle. However, comparing R1 and R2 results, it is visible a discrepancy between both devices performance degradation. This observation suggests that, beyond the electrolyte evaporation, PPy coating degradation can represent another contributing factor for the observed discrepancy. This possibility is supported by the fact that R2 starts with lower performance (low quality coating) and as a smaller variation through cycles, while R1 starts with a higher performance (better PPy coating) but degrades considerable on the first 100 cycles. Furthermore, R2

discharge curves seems straight, with a constant slop, more similar with the CCD results from the woven devices without PPy. With these observations, PPy functionalization and the electrodes woven process shown the need of further optimization to achieve a robust device. Regarding the device cycle stability, due to the electrolyte evaporation could not be sharply evaluated.

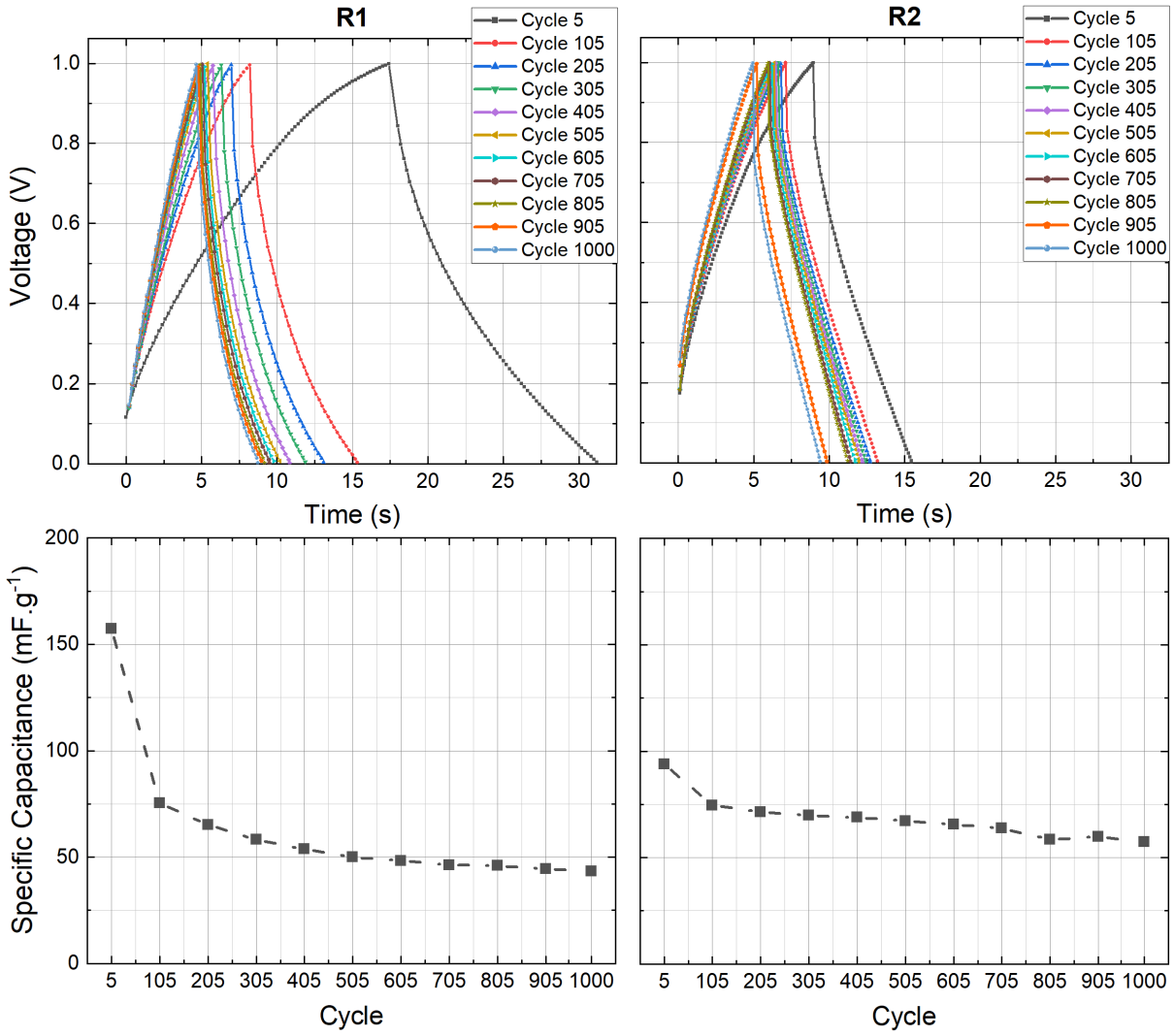

Figure 3.20 - **Top:** Results of the 1000 cycles CCD performed on 2 internal woven replicas, from cycle 5 to cycle 905 with a 100-cycle step and ending on the 1000 cycle. **Bottom:** The correspondent SC estimated for each cycle.

3.4 Mesh like configuration

The final experimented configuration consisted in creating a mesh like structure with carbon threads. This device electrodes and working principle are equivalent to the non-functionalized braid-like device, as described in the *Materials and Methods* subject. **Figure 3.21** shows CV and CCD response of three mesh-like capacitors with different electrodes number (3 CA coated electrodes meshed with 3, 6 and, 12 simple carbon thread electrodes respectively), as well as their estimated capacitance vs charge current. This fabric like approach shown similar CV and CCD results to braid-like non functionalized devices, although with thinner and considerably more tilted CV curves, indicating lower SC values. These characteristics are related to the smaller and uneven contact area, between electrodes, due to its mesh nature. SC values were not estimated for this configuration once the electrodes contributing area, responsible for its electrical behavior, were just the crossing region between electrodes, as shown in **Figure 2.1**, present in *Materials and methods* chapter and the appendix **Figure**

B. 4. This way, estimating its SC, using its electrodes mass, would not result in a valid approximation as in the previous configuration, since most of its electrode's area do not contribute to the desired charge accumulation.

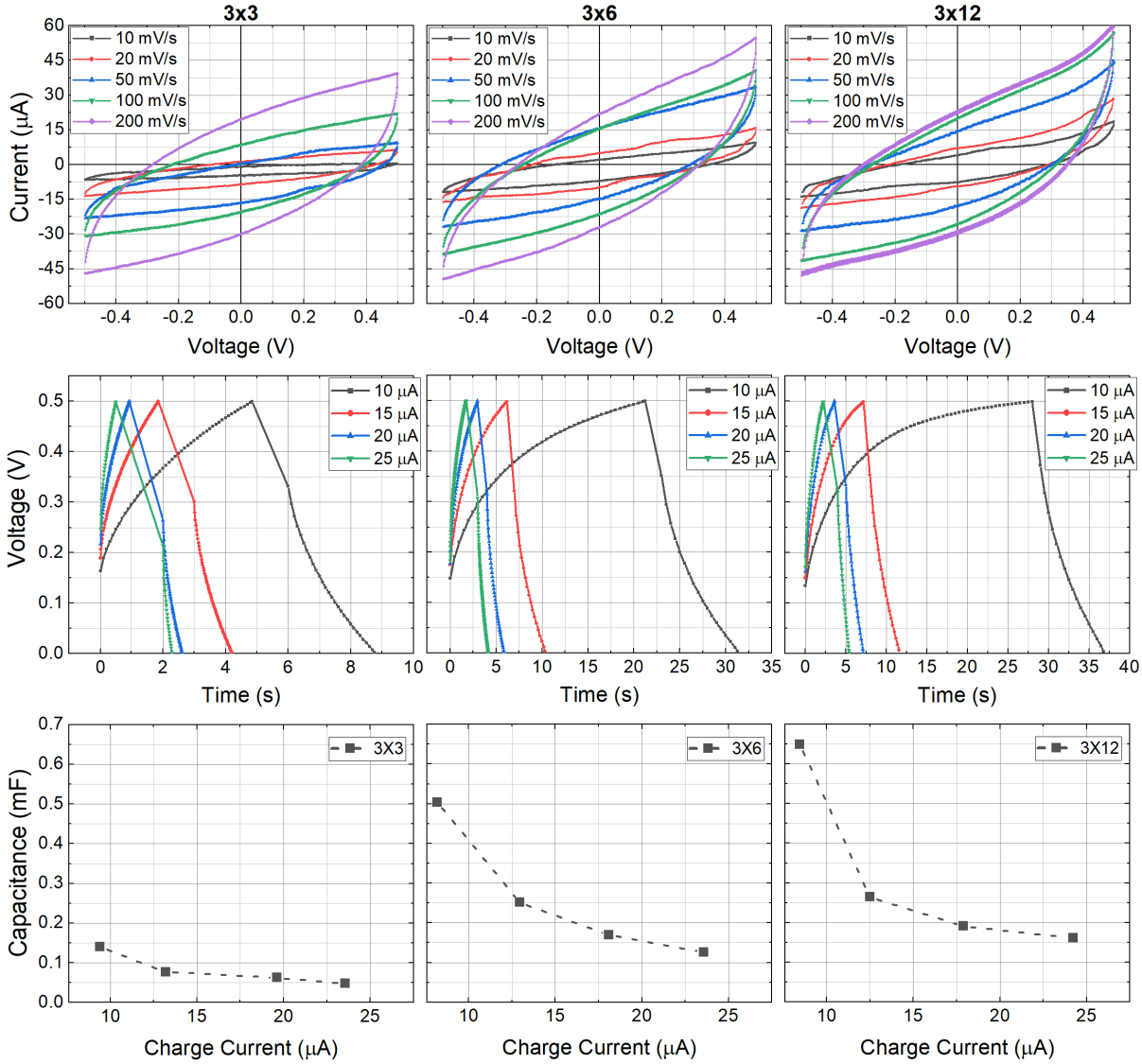

Figure 3.21 - **Top:** CV curves attained from three mesh-like (3x3, 3x6, and 3x12 arrangement) devices experimenting, with SR of 10 mV/s, 20 mV/s, 50 mV/s, 100 mV/s, and 200 mV/s, through a voltage window form -0.5 V to 0.5 V. **Center:** CCD results from the same devices with 10 µA, 15 µA, 20 µA, and 25 µA of charge-discharge current through the same -0.5 V to .05 V voltage window. **Bottom:** Graphical display of the estimated device capacitance vs its charge current for all tested charge-discharge (real) currents.

Nonetheless, considering that only a small area of the 10 cm electrodes was useful, this configuration shown to have potential for future applications due to its simple mesh-like arrangement, that can be adapted to the current industrial textile production methods. Moreover, with a more detailed study and a tighter mesh arrangement, the attained capacitance values can be raised and PPy can be added to the electrodes for further performance enhancement, reaching a higher level of device maturation. However, in this work, the mesh like configuration only made to the preliminary experiments due to its difficult handling, high resource consumption and performance estimation challenges. Nevertheless, mesh-like configuration is presented in this work, for further studies, as a viable approach for directed weaved functional fabric.

4 Conclusions

Throughout the presented work, 1D supercapacitors were successfully assembled and electrical characterized, using cyclic voltammetry and cyclic charge-discharge measurements. Regarding the presented braid-like configuration, it shows to be the most reliable configuration with the average highest estimated specific capacitance values, as displayed in appendix **Table 1** and **Table 3**. Moreover, the braid-like approached, effectively reduce the outer electrode unfolding tendency, promoting the device mechanical stability. However, this new braid-like configuration still presented challenges to be solved, namely, find a better solution for the braiding process that allows wither usable electrode area, reduces the broken filaments problem, and enhance its washing resistance. Furthermore the attained SC values were far from the expectations, being one order of magnitude smaller than the ones presented in *Lima et al.* [1] work. The used method for estimating electrodes mass had a considerable impact on SC calculation, since the charge accumulation phenomenon occurs mostly on electrodes surface. However, to estimate the SC values, it was considered the mass of one full electrode (carbon thread functionalized with PPy), instead of the superficial PPy coating layer mass that effectively holds most of the charge. Yet, the specific capacitance values estimated in this work are in the same scale of magnitude as the ones presented in *Lima et al.* for an asymmetric device, with only the inner electrode functionalized. This suggests that the observed low performance can be related to PPy coating lost on the outer electrode, during assembling and testing processes. Moreover, as refereed in Results and Discussion section, the presented supercapacitor on reference [1] had 11 outer electrode turns, will the ones achieved in this work only had 9. The cellulose acetate coating could have also contributed to the weaker performance, since the CA coating process was extended 1h in comparison to *Lima et al.* process. This increase in time had the objective to ensure a total electrode coating, once using 30 min plus 30 mins process, as described in *Lima et al.* work, the electrode presented sporadically uncoated spots. The use of a different electrospinning equipment for this work probably influenced the referred outcome.

The achieved woven configurations also shown some strengths, namely its simplicity, mechanical stability, and considerable performance, with supercapacitor R3 reaching the highest specific capacitance registered throughout the work, as displayed in **Table 3**. Furthermore, woven functionalized device shown better resistance to washing, in comparison to the braid-like configurations, maintain its CV curves after each washing cycle. Moreover, woven configurations retaining up to 80% of its initial SC in the end of the fifth cycle in contrast to the braid-like configuration that only retained up to 71 % of its initial SC for R2. This is mainly due to the electrode's protection that the internal woven configuration provides, with its electrodes woven inside the felt. The non-functionalized arrangement in series and in parallel shown the possibility of using simpler devices connected to each other to reach higher specifications. Specialty with a more accurate woven process that would allow shorter electrode distance. Nonetheless, this reality can be extended to functionalized devices through a more controlled woven process. On the other hand, the woven process shown to be critical for the device success, being one limiting factor for the woven configurations due to the resulting broken electrode filaments and the occasional PPy strip off. Although not extensively studied, the mesh-like configuration presented a possible application of the studied supercapacitor, in a configuration very similar to industrial garment production. Yet its complex assemble nature and associated high material usage limited its study to a basic demonstration of the concept.

Furthermore, PPy functionalization shown to be the great challenge to reach the desired supercapacitor, since this step greatly influenced the final device SC. Besides all the efforts to achieve a high quality PPy functionalization, the final coating was not very uniform and PPy adhesion to the used carbon yarns was weak, resulting in coating losses during the device handling. This way PPy functionalization on the used carbon threads should be further studied to achieve sharper results. Other verified issue, transversal to all experimented configurations, is the brittleness of the carbon filaments that form the threads. This condition result in some anomalous devices with shorten electrodes and contribute to degrade their performances. Overall, the studies configuration proven to be feasible, having their strengths and weaknesses, whit potential to be further improved. Finally, as displayed in **Table 4**, the presented devices still have a long developing way ahead to compete with the research approaches for wearable supercapacitors, presented in literature. Nonetheless, the difference between the attained

values for SC, E_d, and P_d on this work, in contrast with the ones presented in the literature, can be related with the considered electrode mass for the present work that can be higher than the effective electrode, mass as stated before.

5 Further Perspectives

Despite the remarkable results obtained in the presented document, future research work is needed to solidify the attained conclusions. Starting by the PPy polymerization step, it should be further optimized to obtain more reproductible replicas and different branded carbon yarns should be experimented, with the objective to increase PPy/carbon yarn affinity. Moreover, surface activation treatments (like ozone treatment) cold be applied on the carbon electrodes, before the polymerization step, aiming once again to enhanced PPy/carbon yarn affinity. Electrochemical deposition technique could also be experimented to further control and improve PPy coating uniformity. In terms of the braid like assemble process, its handmade nature shown to be a limiting factor for the achievable device performance. Being so, it could be advantageous to assemble a braiding and/or twisting device, similar to the one presented in reference [4], able to release the resulting twisting strain and achieve a higher number of turns for both configurations. Concerning the supercapacitors electrical characterization, electrical impedance spectroscopy assays should be carried out, before and after the CV and CCD cycles, to better characterize the devices electrical behavior and influence of the said cycles. Furthermore, since flexibility is one of the key characteristics of the presented configurations, supercapacitors bendability should be studied in the future, following the described experiment present on reference [1]. Moreover, cyclic-voltammetry assays with low scan-rate (around 2mV/s) should be performed in other to estimate the functionalized devices specific capacitance values, Ed, and Pd, following the standard parameters presented in literature. Regarding the devices cyclic charge-discharge stability for 1000 cycles, the experiment should be repeated with periodic addictions of electrolyte (for example, adding 25 µL of electrolyte, each 15 min for the braid-like device and 250 µL for the internally woven device each 20 since the second retains the electrolyte better) to effectively describe their cyclic stability. Finally, more device replica of braid-like, woven and mesh-like configurations must be assembled and electrically characterized to prove their reproducibility and define its working characteristic standards.

Bibliography

[1] N. Lima, A. C. Baptista, B. M. M. Faustino, S. Taborda, A. Marques, and I. Ferreira, "Carbon threads sweat-based supercapacitors for electronic textiles," *Sci. Rep.*, vol. 10, no. 1, pp. 1–9, 2020.

[2] C. Callewaert, B. Buysschaert, E. Vossen, V. Fievez, T. Van de Wiele, and N. Boon, "Artificial sweat composition to grow and sustain a mixed human axillary microbiome," *J. Microbiol. Methods*, vol. 103, pp. 6–8, 2014.

[3] N. S. Caetano, T. M. Mata, A. A. Martins, and M. C. Felgueiras, "New Trends in Energy Production and Utilization," *Energy Procedia*, vol. 107, no. September 2016, pp. 7–14, 2017.

[4] H. Sun, Y. Zhang, J. Zhang, X. Sun, and H. Peng, "Energy harvesting and storage in 1D devices," pp. 1–12, 2017.

[5] A. C. Review, J. S. Heo, J. Eom, Y. Kim, and S. K. Park, "Recent Progress of Textile-Based Wearable Electronics : and Applications," vol. 1703034, pp. 1–16, 2018.

[6] Q. Shi, J. Sun, C. Hou, Y. Li, Q. Zhang, and H. Wang, "Advanced Functional Fiber and Smart Textile," *Adv. Fiber Mater.*, no. 0123456789, 2019.

[7] S. Praveen, P. Santhoshkumar, Y. C. Joe, C. Senthil, and C. W. Lee, "3D-printed architecture of Li-ion batteries and its applications to smart wearable electronic devices," *Appl. Mater. Today*, vol. 20, p. 100688, 2020.

[8] J. J. P. C. Rodrigues *et al.*, "Enabling Technologies for the Internet of Health Things," *IEEE Access*, vol. 6, no. 1, pp. 13129–13141, 2018.

[9] P. Torres, "The Augmented Soma Suit : Wearables for Enhanced Somatic Experiences," 2017.

[10] S. Zhai, H. E. Karahan, C. Wang, Z. Pei, L. Wei, and Y. Chen, "1D Supercapacitors for Emerging Electronics: Current Status and Future Directions," *Adv. Mater.*, vol. 32, no. 5, pp. 1–19, 2019.

[11] J. Yang *et al.*, "Heterogeneous graphene/polypyrrole multilayered microtube with enhanced capacitance," *Electrochim. Acta*, vol. 304, 2019.

[12] F. Yi, H. Ren, J. Shan, X. Sun, D. Wei, and Z. Liu, "Wearable energy sources based on 2D materials," *Chem. Soc. Rev.*, vol. 47, no. 9, pp. 3152–3188, 2018.

[13] L. Bach-Toledo, B. M. Hryniewicz, L. F. Marchesi, L. H. Dall'Antonia, M. Vidotti, and F. Wolfart, "Conducting polymers and composites nanowires for energy devices: A brief review," *Mater. Sci. Energy Technol.*, vol. 3, pp. 78–90, 2020.

[14] N. Hillier, S. Yong, and S. Beeby, "The good, the bad and the porous: A review of carbonaceous materials for flexible supercapacitor applications," *Energy Reports*, vol. 6, pp. 148–156, 2020.

[15] Q. Meng, K. Cai, Y. Chen, and L. Chen, "Research progress on conducting polymer based supercapacitor electrode materials," *Nano Energy*, vol. 36, no. April, pp. 268–285, 2017.

[16] S. J. Varma, K. Sambath Kumar, S. Seal, S. Rajaraman, and J. Thomas, "Fiber-Type Solar Cells, Nanogenerators, Batteries, and Supercapacitors for Wearable Applications," *Adv. Sci.*, vol. 5, no. 9, 2018.

[17] Z. Wen *et al.*, “Self-powered textile for wearable electronics by hybridizing fiber-shaped nanogenerators , solar cells , and supercapacitors,” 2016.

[18] M. Chen, Y. Ma, J. Song, C. F. Lai, and B. Hu, “Smart Clothing: Connecting Human with Clouds and Big Data for Sustainable Health Monitoring,” *Mob. Networks Appl.*, vol. 21, no. 5, pp. 825–845, 2016.

[19] K. Kim *et al.*, “Highly Sensitive and Wearable Liquid Metal-Based Pressure Sensor for Health Monitoring Applications: Integration of a 3D-Printed Microbump Array with the Microchannel,” *Adv. Healthc. Mater.*, vol. 8, no. 22, pp. 1–10, 2019.

[20] A. Yu *et al.*, “Core-Shell-Yarn-Based Triboelectric Nanogenerator Textiles as Power Cloths,” *ACS Nano*, vol. 11, no. 12, pp. 12764–12771, 2017.

[21] K. Li, T. Zhao, H. Wang, S. Zhang, and C. Deng, “From 1D nanotube arrays to 2D nanosheet networks on silver-coated textiles: New insights into the factors determining the performance of a core-shell hierarchical structure for wearable supercapacitors,” *J. Mater. Chem. A*, vol. 6, no. 4, pp. 1561–1573, 2017.

[22] Z. Gao, C. Bumgardner, N. Song, Y. Zhang, J. Li, and X. Li, “Cotton-textile-enabled flexible self-sustaining power packs via roll-to-roll fabrication,” *Nat. Commun.*, vol. 7, 2016.

[23] Q. Wang, Y. Ma, X. Liang, D. Zhang, and M. Miao, “Flexible supercapacitors based on carbon nanotube-MnO2 nanocomposite film electrode,” *Chem. Eng. J.*, vol. 371, no. January, pp. 145–153, 2019.

[24] H. Ren *et al.*, “Hierarchical Graphene Foam for Efficient Omnidirectional Solar–Thermal Energy Conversion,” *Adv. Mater.*, vol. 29, no. 38, pp. 1–7, 2017.

[25] Z. Sun *et al.*, “Generalized self-assembly of scalable two-dimensional transition metal oxide nanosheets,” *Nat. Commun.*, vol. 5, no. May, pp. 1–9, 2014.

[26] J. Qiao, X. Kong, Z. X. Hu, F. Yang, and W. Ji, “High-mobility transport anisotropy and linear dichroism in few-layer black phosphorus,” *Nat. Commun.*, vol. 5, pp. 1–7, 2014.

[27] W. Liu *et al.*, “3D Porous Sponge-Inspired Electrode for Stretchable Lithium-Ion Batteries,” *Adv. Mater.*, vol. 28, no. 18, pp. 3578–3583, 2016.

[28] A. Ramadoss, K. Y. Yoon, M. J. Kwak, S. I. Kim, S. T. Ryu, and J. H. Jang, “Fully flexible, lightweight, high performance all-solid-state supercapacitor based on 3-Dimensional-graphene/graphite-paper,” *J. Power Sources*, vol. 337, pp. 159–165, 2017.

[29] X. Cao, Z. Yin, and H. Zhang, “Three-dimensional graphene materials: Preparation, structures and application in supercapacitors,” *Energy Environ. Sci.*, vol. 7, no. 6, pp. 1850–1865, 2014.

[30] Y. Wang *et al.*, “3D-Printed All-Fiber Li-Ion Battery toward Wearable Energy Storage,” *Adv. Funct. Mater.*, vol. 27, no. 43, pp. 1–8, 2017.

[31] X. Chen, R. Paul, and L. Dai, “Carbon-based supercapacitors for efficient energy storage,” *Natl. Sci. Rev.*, vol. 4, no. 3, pp. 453–489, 2017.

[32] R. A. Huggins and S. Edition, *Energy Storage*, 2nd ed. Springer, 2016.

[33] D. Halliday, R. Resnick, and G. H. Bowen, *Fundamentals of Physics*, 10th ed., vol. 25, no. 4. 1972.

[34] Poonam, K. Sharma, A. Arora, and S. K. Tripathi, “Review of supercapacitors: Materials and devices,” *J. Energy Storage*, vol. 21, no. January, pp. 801–825, 2019.

[35] Y. Kado, Y. Soneda, H. Hatori, and M. Kodama, “Advanced carbon electrode for

electrochemical capacitors," *J. Solid State Electrochem.*, vol. 23, no. 4, pp. 1061–1081, 2019.

[36] H. Butt, K. Graf, and M. Kappl, *Physics and Chemistry of Interfaces*. 2003.

[37] X. Liu, S. Chen, J. Pu, and X. Wang, "A Flexible All-Solid-State Micro Supercapacitor and Its Application in Electrostatic Energy Management System," *J. Microelectromechanical Syst.*, vol. 25, no. 5, pp. 929–936, 2016.

[38] H. S. Williams, "A History of Science, Vol. II by Henry Smith Williams," 2009. [Online]. Available: https://www.gutenberg.org/files/1706/1706-h/1706-h.htm. [Accessed: 19-May-2021].

[39] J. Noh, C. M. Yoon, Y. K. Kim, and J. Jang, "High performance asymmetric supercapacitor twisted from carbon fiber/MnO2 and carbon fiber/MoO3," *Carbon N. Y.*, vol. 116, 2017.

[40] M. Toupin, T. Brousse, and D. Bélanger, "Charge storage mechanism of MnO2 electrode used in aqueous electrochemical capacitor," *Chem. Mater.*, vol. 16, no. 16, pp. 3184–3190, 2004.

[41] A. Noori, M. F. El-Kady, M. S. Rahmanifar, R. B. Kaner, and M. F. Mousavi, "Towards establishing standard performance metrics for batteries, supercapacitors and beyond," *Chem. Soc. Rev.*, vol. 48, no. 5, pp. 1272–1341, 2019.

[42] N. R. C. Lima, "Development of functional fibers for wearable applications," 2018.

[43] V. L. Pushparaj *et al.*, "Sciences of the USA 13574-13577 PNAS," vol. 104, no. 34, pp. 1–4, 2007.

[44] L. Manjakkal, A. Pullanchiyodan, N. Yogeswaran, E. S. Hosseini, and R. Dahiya, "A Wearable Supercapacitor Based on Conductive PEDOT:PSS-Coated Cloth and a Sweat Electrolyte," *Adv. Mater.*, vol. 32, no. 24, 2020.

[45] Y. M. Fan, W. L. Song, X. Li, and L. Z. Fan, "Assembly of graphene aerogels into the 3D biomass-derived carbon frameworks on conductive substrates for flexible supercapacitors," *Carbon N. Y.*, vol. 111, pp. 658–666, 2017.

Appendix A - Supplementary figures

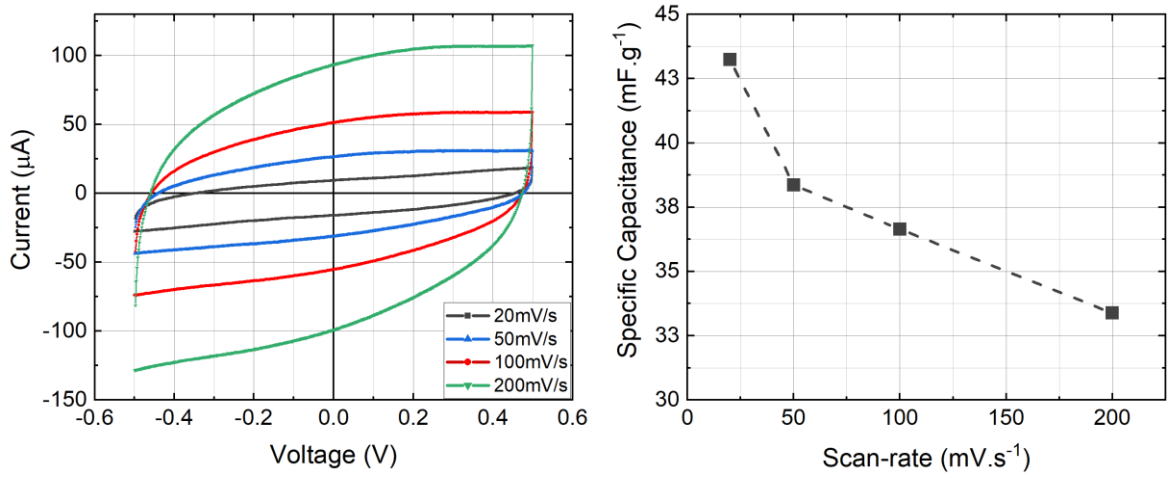

Figure A. 1- Left: Resulting CV curves from 1D device, braid-like, with 10 turns, using scan-rates of 20 mV/s, 50 mV/s, 100 mV/s and 200 mV/s. **Right:** Scan-rate vs specific capacitance results.

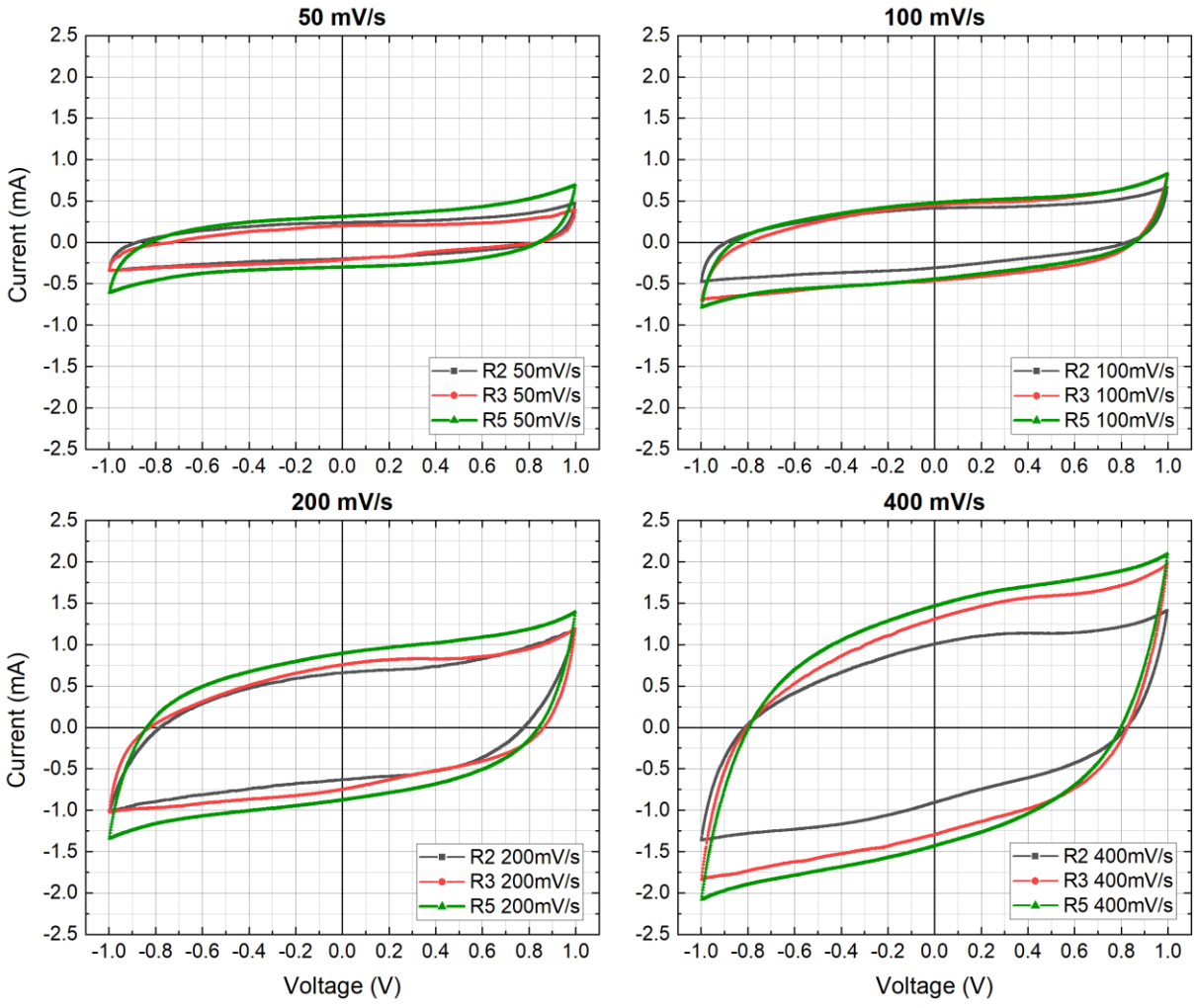

Figure A. 2 - Comparison between the obtained CV curves from the 3 braid-like replicas emphasizing their similarity within each tested scan-rate.

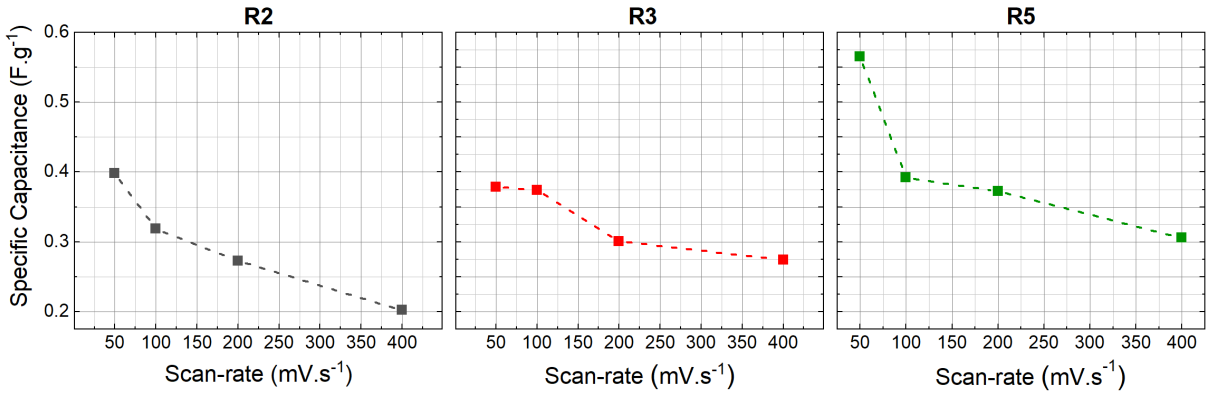

Figure A. 3 - SR vs SC of 1D braid-like devices, namely R2, R3 and R5. This time using the cycle 2 of the CV with 50 mV/s, to estimate the SC of R3.

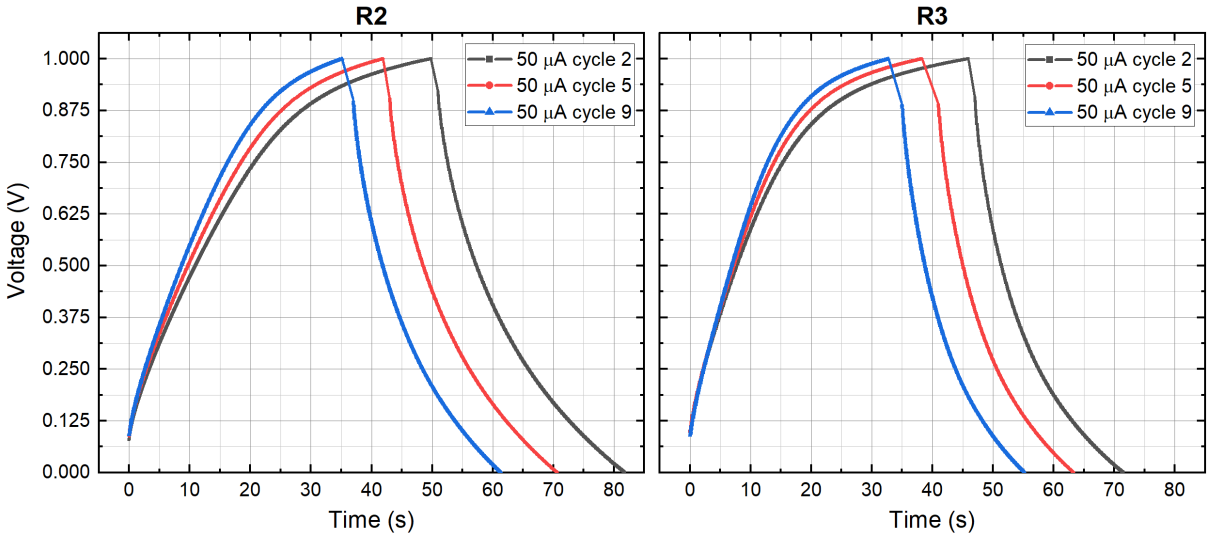

Figure A. 4 - Illustration of the difference between charge-discharge cycles in the same CCD assay. Particularly, between the 2nd, the 5th, and the 9th cycle of 50 µA CCD assay, on braid-like device R2 and R3 replicas.

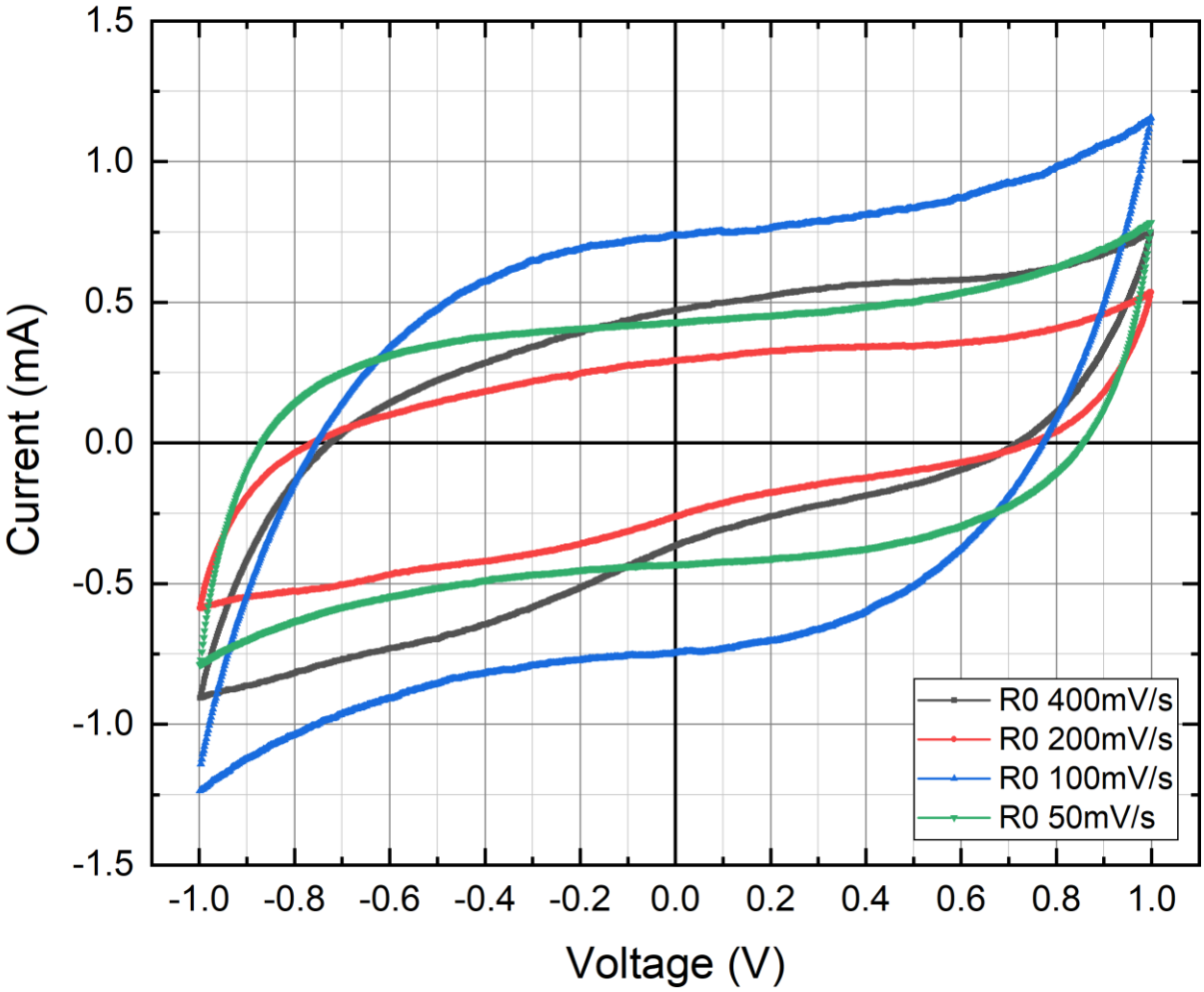

Figure A. 5 - Anomalous CV results from R0, 1D braid-like device, performed after testing the device sweep voltage window limit. Comparison between the tested scan-rates (50 mV/s, 100 mV/s, 200 mV/s and 400 mV/s) using a sweep voltage window from -1 V to 1 V.

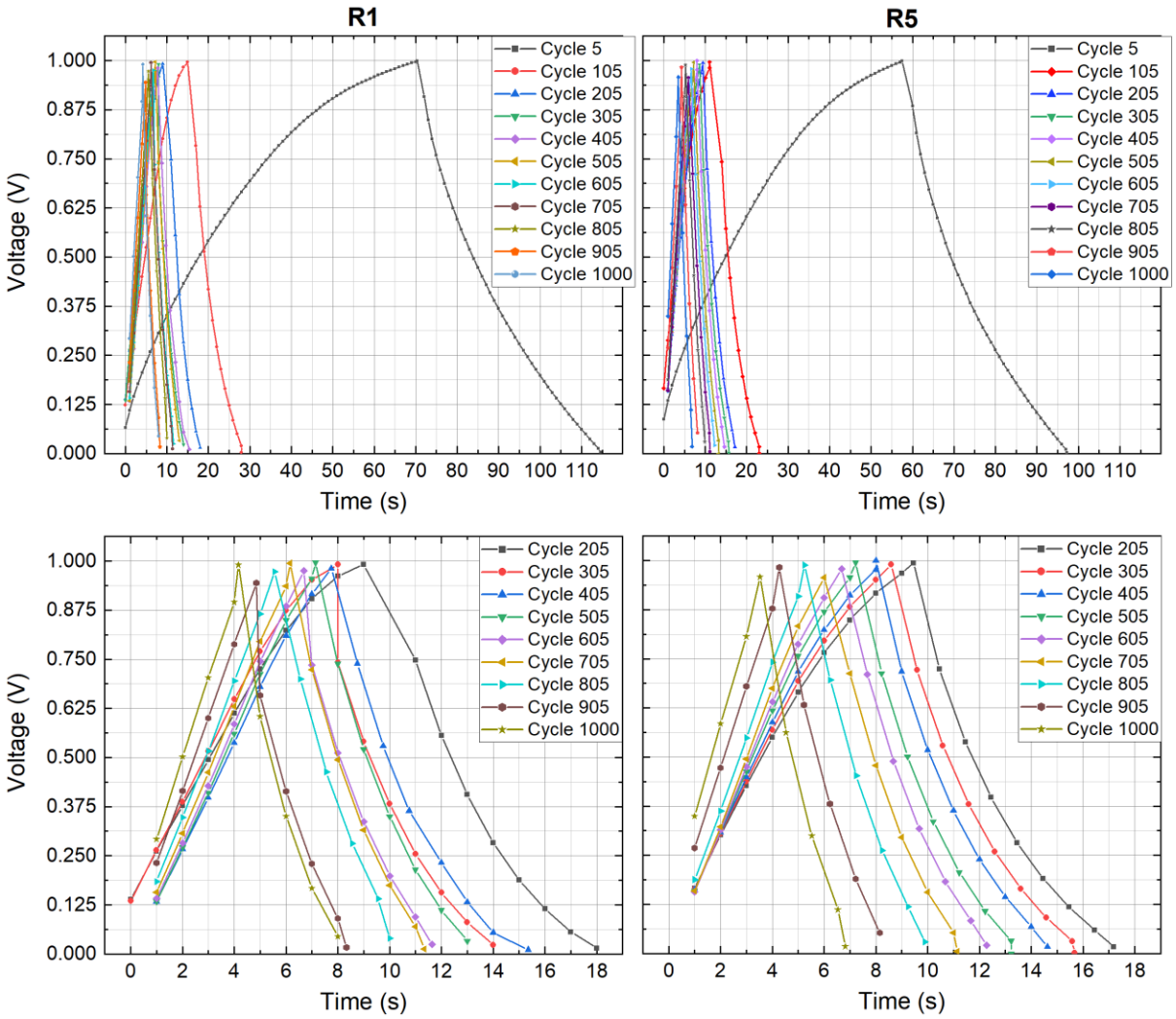

Figure A. 6 - CCD results from the 1000 cycles experiment on the braid-like configuration (R1 and R5). The top figures display the 1000 CCD cycles, from cycle 5 to cycle 905 with 100 cycles step in between and ends with the 1000. The bottom figures display a close up from the 205th cycle to the 1000th cycle.

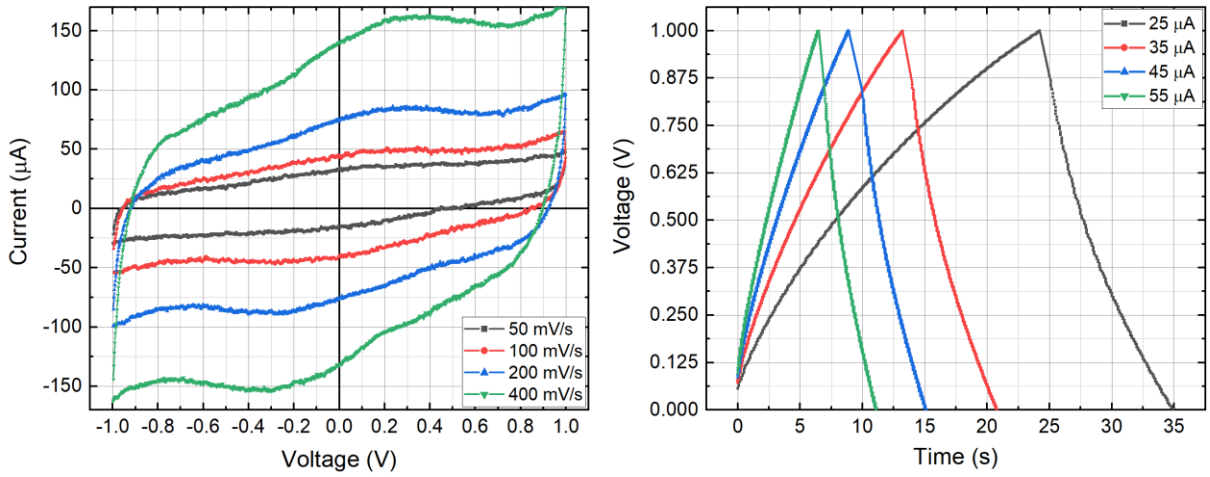

Figure A. 7 - CV (left) and CCD (right) results from one internally woven, carbon only electrode devices, connected in series, and tested with a voltage widow from -1 V to 1 V with scan-rates of 50 mV/s, 100 mV/s, 200 mV/s, and 400 mV/s for CV experiment. Regarding the CCD assays, a charging voltage from 0 V to 1V, with charge-discharge currents of 25 µA, 35 µA, 45 µA, and 55 µA were used.

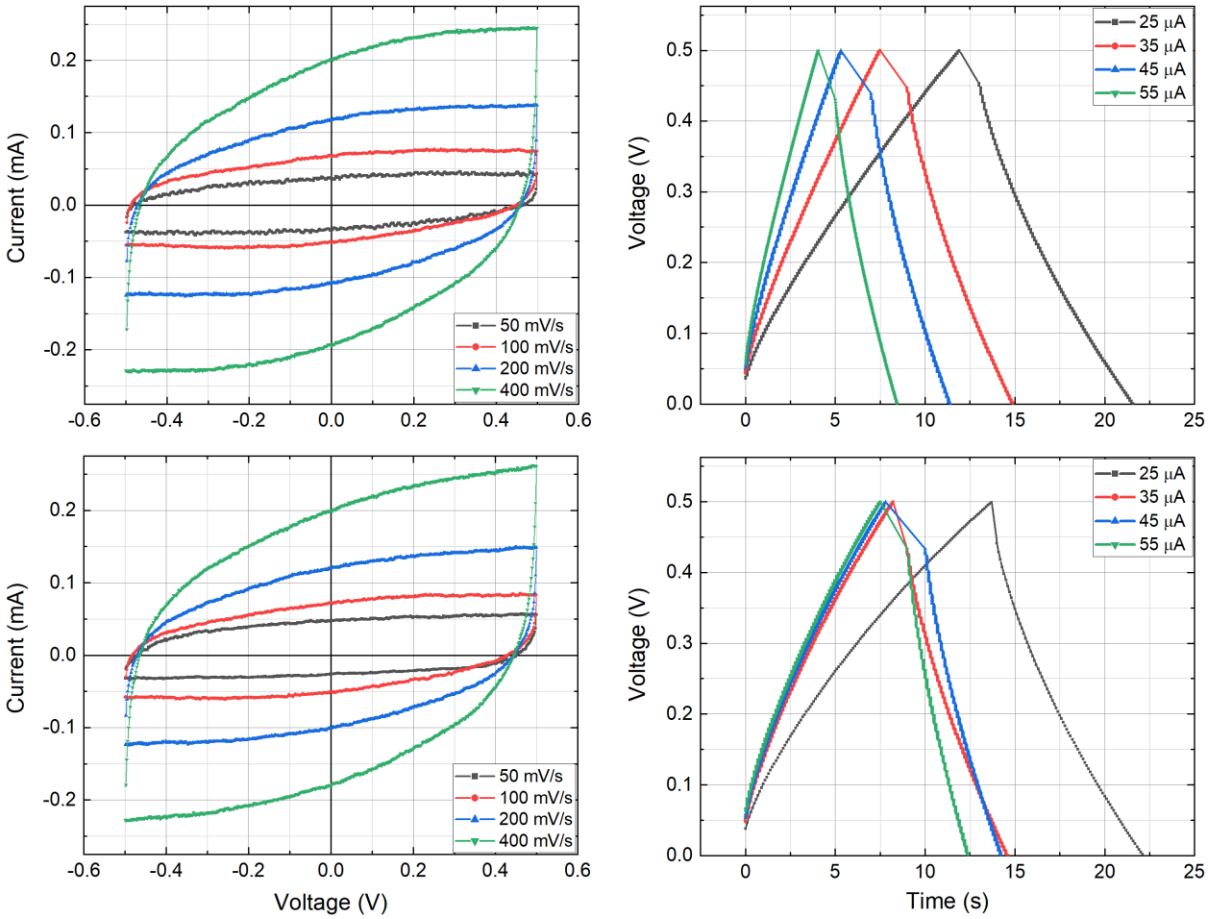

Figure A. 8 - Comparison between the CV and CCD results obtained with the first configuration (top graphics) and the second configuration (bottom graphics) of two, internally woven, carbon only electrode capacitors, connected in parallel.

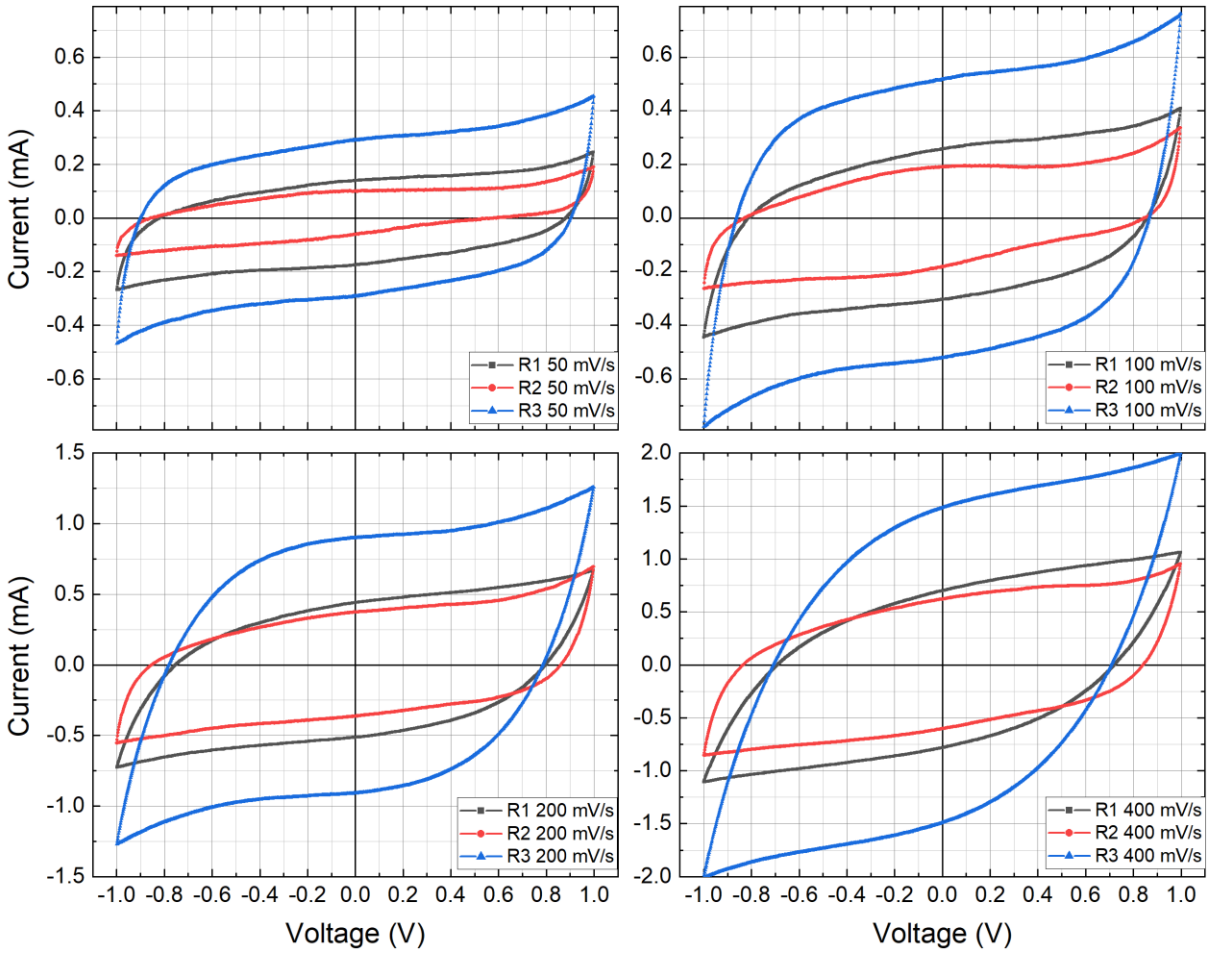

Figure A. 9 - Comparison between the four tested SR, on the internally woven replicas, with functionalized electrodes, 0.3 cm apart.

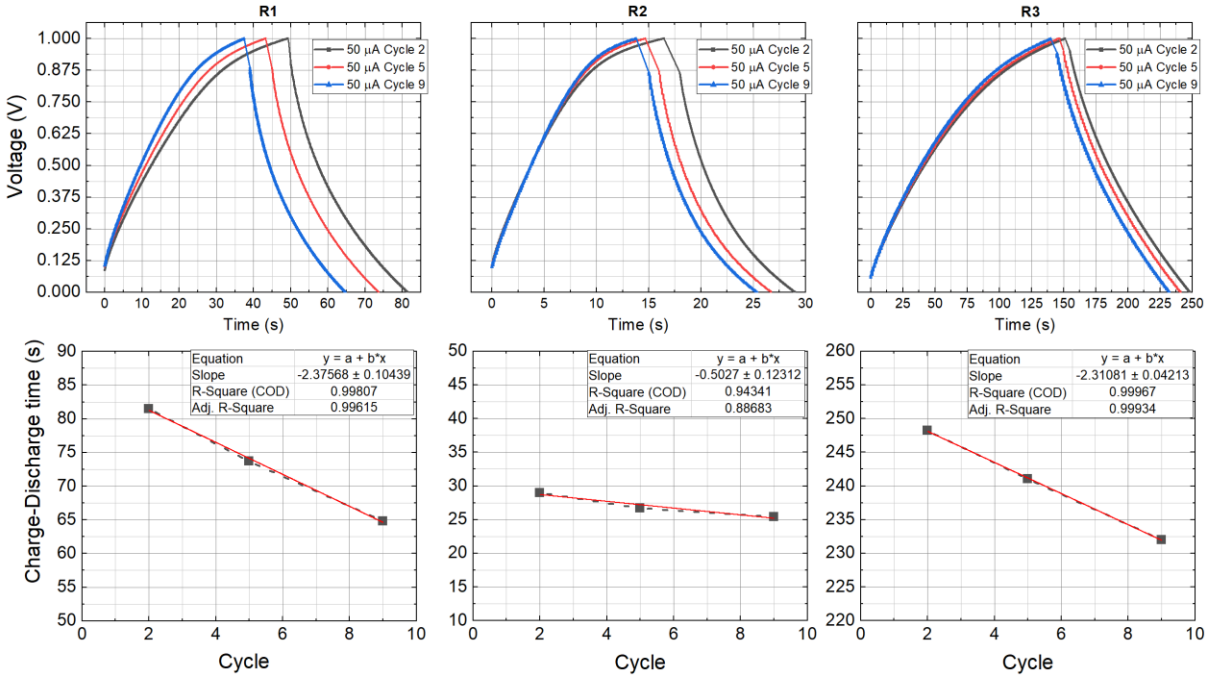

Figure A. 10 - CCD graphics of functionalized internally woven replicas from the 2nd, 5th, and 9th cycle of 50 uA Charge-discharge run (top). Cycle vs charge-discharge time graphics with the respective linear regression(bottom).

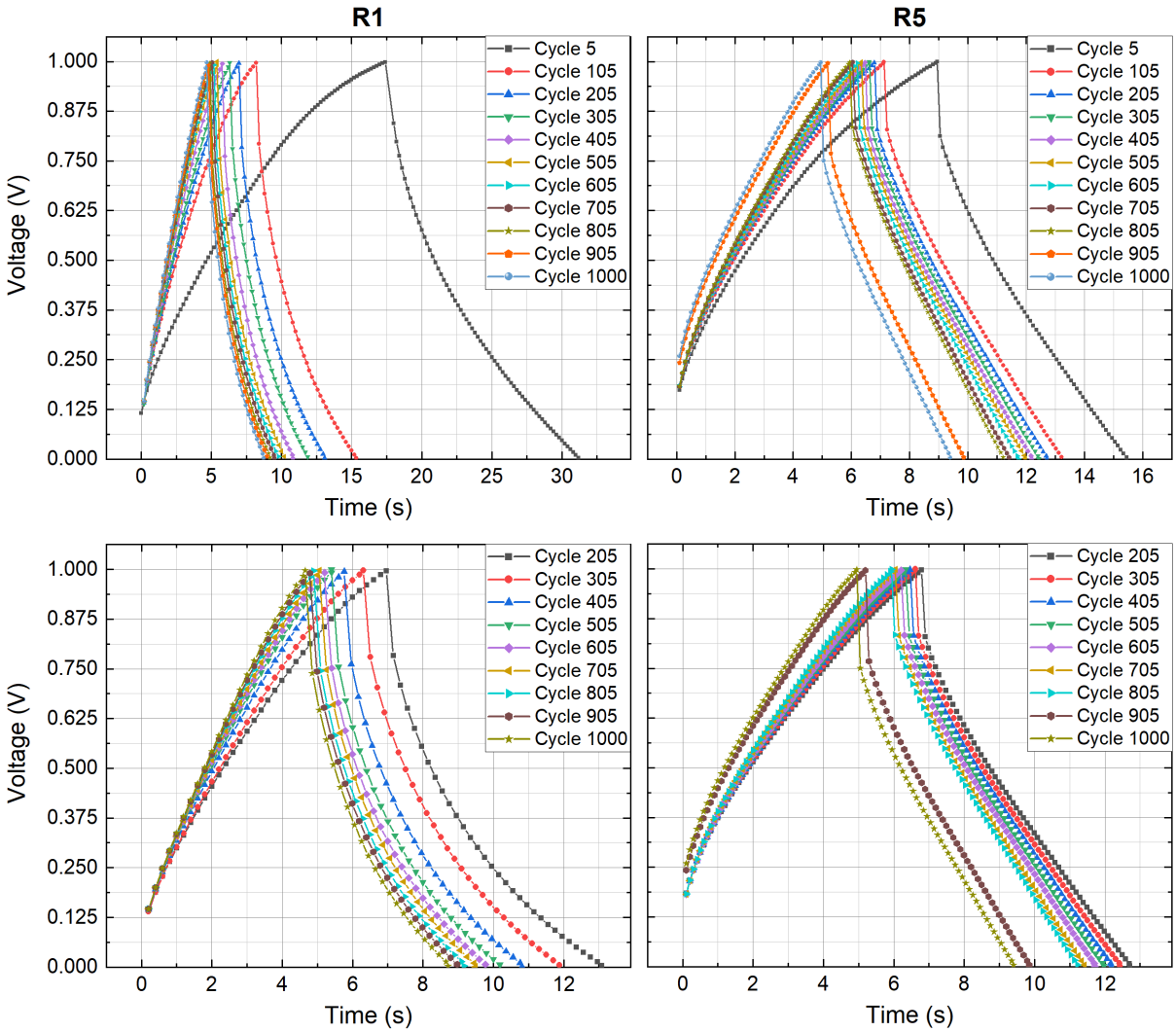

Figure A. 11 - CCD results from the 1000 cycles experiment on the woven configuration (R1 and R2). The top figures display the 1000 CCD cycles, from cycle 5 to cycle 905 with 100 cycles step in between and ends with the 1000. The bottom figures display a close up from the 205th cycle to the 1000th cycle.

Appendix B – Supplementary Images

Figure B. 1 - left: Photo of the frame used to support the carbon threads during electrospining. **Right:** photo of a similar elecreospining setup from [42].

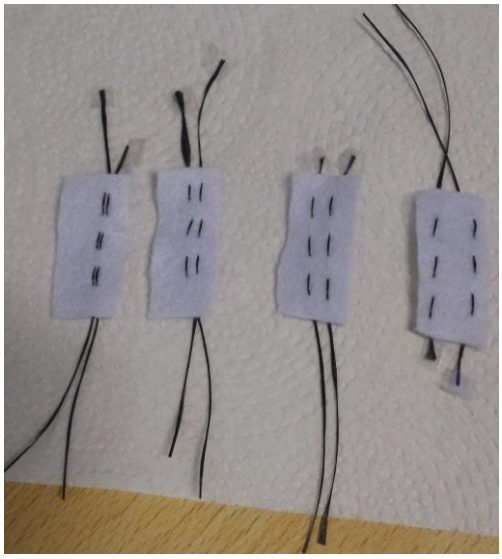

Figure B. 2 - Photo of the 4 electrodes distance tested on the parallel external woven device, namely 0.1 cm to 1 cm from left to right. The featured devices present a half carbon thread electrode.

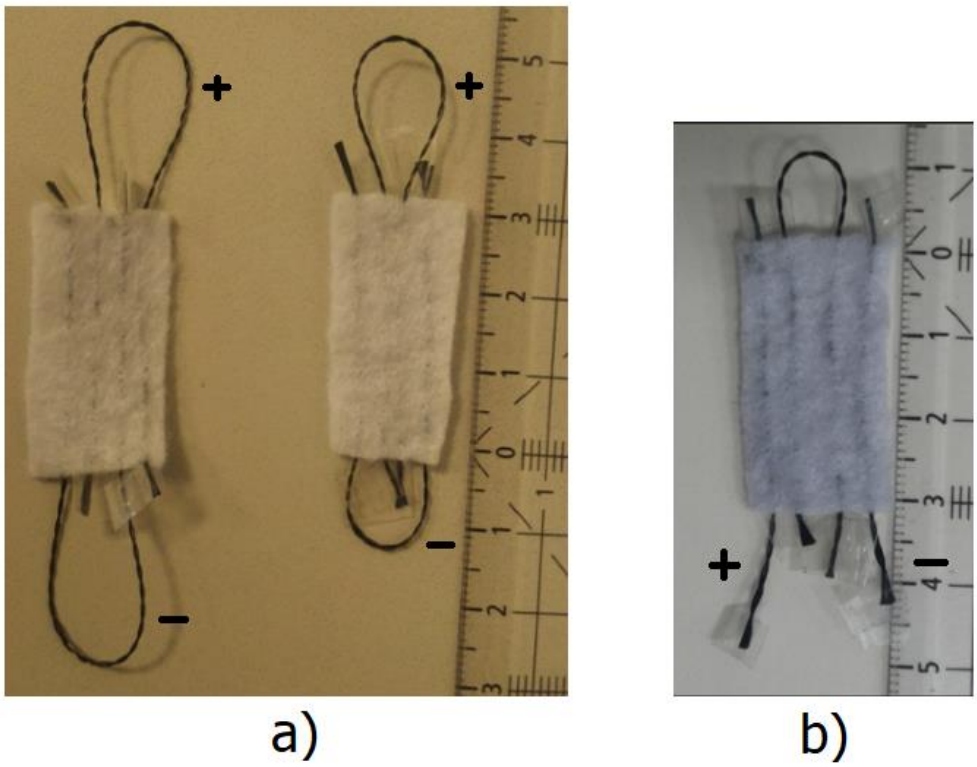

Figure B. 3 - Pictures of a) the 4 threaded devices with parallel arrangement being the left on the firs to be tested and the right one the second and b) series arrangement.

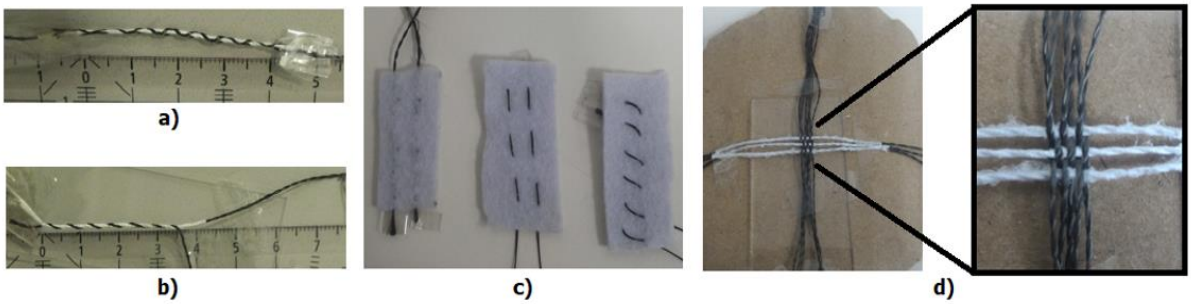

Figure B. 4 - Photographs of 1D configuration devices. Braid-like and twisted-like configurations represented on image **a)** and **b)** respectively. Woven configurations (internal, parallel and crossed) are peresent in image **c)** and mesh-like configuration is displyed on image **d)**.

Appendix C – Supplementary Tables

Table 1 - Specific capacitance results from 1D supercapacitors without PPy functionalization.

	Without PPy functionalization	
Braid-Like Supercapacitors	Scan-Rate ($mV.s^{-1}$)	Specific Capacitance ($F.g^{-1}$)
9 Turns	10	0.062
	20	0.035
	50	0.031
	100	0.028
	200	0.023
10 Turns	20	0.043
	50	0.038
	100	0.037
	200	0.033
Externally Woven Electrode Supercapacitors	Scan-Rate ($mV.s^{-1}$)	Specific Capacitance ($F.g^{-1}$)
0.3 cm	10	0.02
	20	0.019
	50	0.017
	100	0.014
	200	0.011
Internally Woven Electrode Supercapacitors	Scan-Rate ($mV.s^{-1}$)	Specific Capacitance ($F.g^{-1}$)
0.3 cm	10	0.06
	20	0.049
	50	0.038
	100	0.037
	200	0.033
0.5 cm	10	0.062
	20	0.055
	50	0.043
	100	0.034
	200	0.032
1 cm	50	0.032
	100	0.027
	200	0.025

Table 2 - Specific capacitance results of the internally woven devices connected in series and parallel, without PPY.

	Scan-Rate ($mV.s^{-1}$)	**Specific Capacitance ($F.g^{-1}$)**
0.3 cm connected in parallel 1	50	0.061
	100	0.05
	200	0.048
	400	0.042
0.3 cm connected in parallel 2	50	0.055
	100	0.048
	200	0.043
	400	0.038
0.3 cm connected in series	50	0.035
	100	0.032
	200	0.025
	400	0.023

Table 3 - Specific capacitance results from the 1D supercapacitors with PPy functionalization.

	Specific Capacitance ($F.g^{-1}$)			
Replicas	**Braid-like supercapacitors**		**Internally woven supercapacitors**	
R1			Scan-Rate ($mV.s^{-1}$)	Specific Capacitance ($F.g^{-1}$)
			50	0.263
			100	0.242
			200	0.207
			400	0.172
R2	Scan-Rate ($mV.s^{-1}$)	Specific Capacitance ($F.g^{-1}$)	Scan-Rate ($mV.s^{-1}$)	Specific Capacitance ($F.g^{-1}$)
	50	0.398	50	0.184
	100	0.319	100	0.177
	200	0.273	200	0.195
	400	0.202	400	0.159
R3	Scan-Rate ($mV.s^{-1}$)	Specific Capacitance ($F.g^{-1}$)	Scan-Rate ($mV.s^{-1}$)	Specific Capacitance ($F.g^{-1}$)
	50	0.318	50	0.616
	100	0.374	100	0.532
	200	0.301	200	0.448
	400	0.274	400	0.391
R5	Scan-Rate ($mV.s^{-1}$)	Specific Capacitance ($F.g^{-1}$)		
	50	0.565		
	100	0.392		
	200	0.372		
	400	0.306		

Table 4 - Brief resume and comparison of some results obtain from similar investigated supercapacitors.

Electrode materials	**Working mechanism / type**	**SC (F. g^{-1})**	**E_d (Wh. kg^{-1})**	**P_d (kW. kg^{-1})**	**Ref.**
Carbon thread / PPy	Hybrid / symmetric	2.3	0.386	46.4	[1]
CNT-MnO_2	Hybrid/asymmetric	323.9 @ 1.9A.g^{-1}	27.14	571.3	[23]
Carbon thread / PPy	Hybrid / symmetric	0.57	0.01	1.6	*
CNT	EDL / symmetric	22	20	1500	[43]
PEDOT: PSS	Hybrid / symmetric	5.65	1.36	0.33	[44]
Co-Al LDH/ACT//ACT/ graphene	Hybrid / asymmetric	145.8	55.04	5.4	[22]
NCCF-rGO	Hybrid / symmetric	225 @ 1 A.g^{-1}	20	4	[45]
Carbon thread / PPy	Hybrid / symmetric	0.62	0.06	2.26	*

* - This work

CNT-MnO_2: Carbon nano tube-MnO_2 nano nanosheet composite film.

CNT: Carbon nanotubes.

PEDOT: PSS: Poly 3,4-ethylenedioxythiophene : polystyrenesulfonate.

NCCF-rGO: N-doping cotton-derived carbon frameworks-reduction of graphene oxide.

Co-Al LDH/ACT//ACT/ graphene: cobalt-aluminum layered double hydroxides / activated cotton textile // activated cotton textile / graphene.